V-ATPase V_1 Sector Is Required for Corpse Clearance and Neurotransmission in *Caenorhabditis elegans*

Glen G. Ernstrom,* Robby Weimer,*,[1] Divya R. L. Pawar,* Shigeki Watanabe,* Robert J. Hobson,* David Greenstein,† and Erik M. Jorgensen*,[2]

*Howard Hughes Medical Institute, Department of Biology, University of Utah, Salt Lake City, Utah 84112-0840 and †Department of Genetics, Cell Biology, and Development, University of Minnesota, Minneapolis, Minnesota 55455-0465

ABSTRACT The vacuolar-type ATPase (V-ATPase) is a proton pump composed of two sectors, the cytoplasmic V_1 sector that catalyzes ATP hydrolysis and the transmembrane V_o sector responsible for proton translocation. The transmembrane V_o complex directs the complex to different membranes, but also has been proposed to have roles independent of the V_1 sector. However, the roles of the V_1 sector have not been well characterized. In the nematode *Caenorhabditis elegans* there are two V_1 B-subunit genes; one of them, *vha-12*, is on the X chromosome, whereas *spe-5* is on an autosome. *vha-12* is broadly expressed in adults, and homozygotes for a weak allele in *vha-12* are viable but are uncoordinated due to decreased neurotransmission. Analysis of a null mutation demonstrates that *vha-12* is not required for oogenesis or spermatogenesis in the adult germ line, but it is required maternally for early embryonic development. Zygotic expression begins during embryonic morphogenesis, and homozygous null mutants arrest at the twofold stage. These mutant embryos exhibit a defect in the clearance of apoptotic cell corpses in *vha-12* null mutants. These observations indicate that the V_1 sector, in addition to the V_o sector, is required in exocytic and endocytic pathways.

ONE role of vacuolar-type proton ATPases (V-ATPase) is to acidify organelles in secretory and endocytic pathways (Mellman *et al.* 1986; Futai *et al.* 2000; Forgac 2007). The V-ATPase is composed of two substructures: a catalytic domain of eight different subunits called the V_1 sector and a membrane-anchored set of subunits called the V_o sector (Figure 1A). Both sectors are required for acidification of cellular organelles; however, genetic analysis suggests that the V_o domain may have an additional role in promoting membrane fusion (Peters *et al.* 2001; Hiesinger *et al.* 2005; Liégeois *et al.* 2006; Sun-Wada *et al.* 2006; Peri and Nüsslein-Volhard 2008; Di Giovanni *et al.* 2010; Williamson *et al.* 2010; Strasser *et al.* 2011). To distinguish the roles of acidification and potential additional roles of the V-ATPase, it is particularly important to identify the functions of the catalytic V_1 sector.

The differential expression and localization of specialized V_1 sector subunits suggest that the proton pump could be adopted for different purposes (Toei *et al.* 2010). For example, in mammals different B isoforms of the V_1 sector are localized to either the cell surface or internal membranes. The B1 isoform is localized to the surface of specialized kidney, inner ear, and vas deferens epithelial cells where it pumps protons into the extracellular space, whereas the B2 subunit is typically associated with endosomes and pumps protons into the lumen of organelles (Brown *et al.* 2009). Consistent with the epithelial localization of B1 subunits, mutations in the B1 surface isoform are linked to renal tubule acidosis and deafness in humans (Karet *et al.* 1999; Stover *et al.* 2002; Hahn *et al.* 2003; Vargas-Poussou *et al.* 2006; Gil *et al.* 2007; Fuster *et al.* 2008).

However, a rigid B-subunit specialization does not seem to be common in all animals. The mouse genome also encodes two B subunits. But unlike humans, mutation of the apical B1 subunit in mice does not result in deafness or kidney dysfunction (Dou *et al.* 2003; Finberg *et al.* 2005). The B2 subunit, normally localized to endosomes, can partially compensate for the loss of B1 subunits (Păunescu *et al.* 2007),

doi: 10.1534/genetics.112.139667
Manuscript received July 15, 2011; accepted for publication February 29, 2012
Supporting information is available online at http://www.genetics.org/content/suppl/2012/03/16/genetics.112.139667.DC1.
Sequence data from this article have been deposited with the NCBI Data Libraries under accession nos. NM_076310.6 and NP_508711.1.
[1]Present address: Biomedical Imaging Group, Department of Neuroscience, Genentech, South San Francisco, CA 94080-4918.
[2]Corresponding author: Howard Hughes Medical Institute, Department of Biology, 257 S. 1400 E., University of Utah, Salt Lake City, UT 84112-0840. E-mail: jorgensen@biology.utah.edu

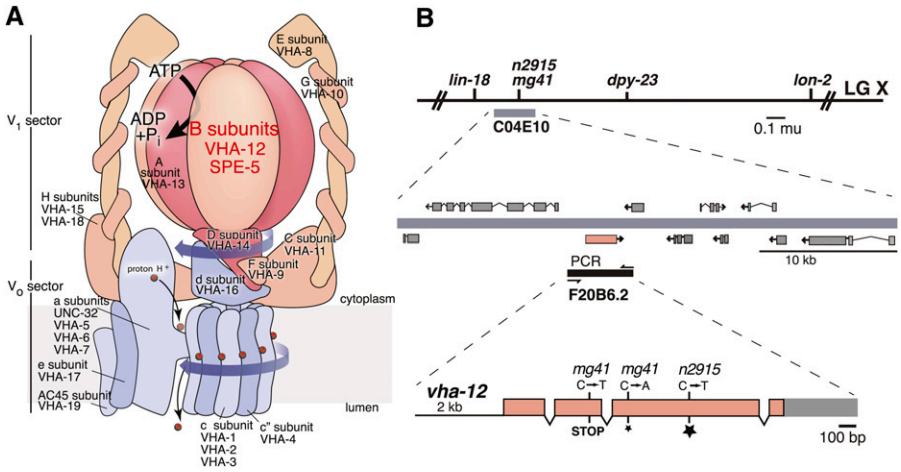

Figure 1 Molecular analysis of the *vha-12* locus. (A) *C. elegans* V-ATPase. The *C. elegans* genome contains homologs of each of the 14 unique vertebrate subunits of the V-ATPase (S. K. Lee *et al.* 2010) (http://www.wormbase.org, release WS224, April 3, 2011). The V_1 sector is shaded orange, and the V_o sector is shaded blue. Four subunits have multiple isoforms; the V_1 subunits B and H have two isoforms, the V_o *a* subunit has four isoforms, and the V_o c subunit has three isoforms. (B) *vha-12* cloning. (Top) Genetic map: mapping and rescue of the *n2915* and *mg41* mutations. The *n2915* mutation was mapped between *lin-18* and *dpy-23* loci. (Middle) Physical map: cosmid C04E10 rescued the *n2915* locomotion defect and contains the coding region for 10 genes. A 5-kb PCR amplification of F20B6.2 was sufficient to completely rescue *vha-12(n2915)* mutants. (Bottom) Sequencing the corresponding region in *vha-12(n2915)* adults and in arrested *vha-12(mg41)* mutant embryos identified the nucleotide changes corresponding to nonsense (stop) and missense (stars) mutations.

suggesting that B-subunit specialization is not universal. Only one B-subunit gene is encoded in the *Drosophila* genome, suggesting that there is no specialization of subunits (Du *et al.* 2006). The fly VHA55 protein is localized on internal membranes as well as on the apical surface on the kidney-like Malpighian tubules, consistent with acidification of organelles and proton extrusion (Du *et al.* 2006). In contrast to B1 mutations in mice, mutations in *vha55* are larval lethal (Davies *et al.* 1996). Thus, mutations in B-subunit genes in mice and flies exhibit two phenotypic extremes: they are nearly wild type or lethal.

The genome of the nematode *Caenorhabditis elegans* encodes two B-subunit genes, called *vha-12* and *spe-5*, as well as multiple genes for other V-ATPase subunits (Figure 1A). To investigate whether these B-subunit genes have specialized functions, we and the authors of the accompanying article in this issue (Gleason *et al.* 2012) have cloned and characterized mutations in each of these loci. We isolated a null allele and a missense allele in the *vha-12* locus, which is on the X chromosome. The missense allele allowed us to examine the effects of impaired V_1 V-ATPase in adult cells. The VHA-12 B subunit is required for acidification of synaptic vesicles and the release of normal levels of neurotransmitter from adult neurons. VHA-12 is also required maternally for early embryogenesis and is required zygotically during morphogenesis. We also show a previously unrecognized role of the catalytic B subunit in the clearance of apoptotic cell corpses in embryos. *vha-12* is thus required broadly, whereas *spe-5* is required only during spermiogenesis (Gleason *et al.* 2012). Together these articles suggest that B-subunit diversity in *C. elegans* may have arisen to escape X chromosome inactivation rather than to provide functional diversity for the V-ATPase proton pump.

Materials and Methods

Strains and alleles

C. elegans strains were cultured using standard methods. The wild type is N2 Bristol (Brenner 1974).

Reference strains: MT7907 *vha-12(n2915sd) X* is a viable mutation isolated in an EMS screen for jerky uncoordinated mutants and outcrossed to N2 four times. GR1029 *lon-2 (e678) let-44(mg41) X*; *mnDp31* is a recessive X-linked embryonic lethal mutation. Briefly, *lon-2* males were mutagenized with EMS and crossed to *unc-20(e112) X* animals. Coordinated cross-progeny were individually screened for the absence of the *lon-2(e678)* X-linked marker in the second filial generation. The lethal mutation *mg41* was outcrossed seven times to N2 and balanced using the free duplication, *mnDp31*. CB189 *unc-32(e189) III* is a mutation in subunit *a* of the V_o sector (Pujol *et al.* 2001).

Rescuing strains: MT7907 *vha-12(n2915sd) X* was rescued by microinjection of DNA from single genes contained in the rescuing cosmid C04E10. The *vha-12* gene was amplified from genomic DNA using oligonucleotides oRW025 and oRW026 to generate a 5-kb PCR fragment (see below). Transformants were identified by co-injection of 20 ng/μl plasmid pEK1[*lin-15(+)*] into EG7341 *vha-12(n2915) lin-15(n765ts) X* (Clark *et al.* 1994). Two of two *lin-15(+)* lines were rescued for the Vha-12 Unc phenotype {EG2371 *vha-12(n2915sd) lin-15(n765ts) X*; *oxEx397[vha-12(+)*; *lin-15 (+)]*}. The 5-kb rescuing PCR fragment was subcloned to generate plasmid pRW05. pRW05 was microinjected into MT7907 *vha-12(n2915sd)* to generate EG3250 *vha-12 (n2915sd)*; *oxEx552 [vha-12(+) pRW05* (2 ng/μl); *Pmyo-3::GFP* (10 ng/μl); *Bluescript* (76 ng/μl)*]* for quantitative analyses of rescue. Embryonic lethality of *vha-12(mg41)* was rescued by injecting GR1029 with the *vha-12(+)* pRW05 plasmid to produce EG3249 *lon-2(e678) vha-12(mg41) X*; *oxEx551[vha-12(+) pRW05* (2 ng/μl); *Pmyo-3::GFP* (10 ng/μl); *Bluescript* (76 ng/μl)*]*. To perform mosaic analysis we generated a strain that contained a rescuing *vha-12 (+)* gene array that expresses GFP under the control of an early developmental promoter. The *vha-12(+)* rescuing plasmid was injected into GR1029 to generate strain EG7188 *lon-2(e678) vha-12(mg41)*; *oxEx1703[vha-12(+)*

pRW05 (0.5 ng/μl); *pCFJ420 Peft-3*::*GFP*::*HIS-58 (histone H2B)* (10 ng/μl); *Punc-122*::*GFP* (60 ng/μl) *coelomocyte marker*; *Promega DNA ladder* (32.5 ng/μl)*]*.

Transcriptional reporter: The transcriptional reporter strain was EG2410 *lin-15(n765ts) X*; *oxEx192* [*Pvha-12*::*NLS*::*GFP*; *lin-15(+)*].

Synaptic marker strains: Synaptic varicosities in a subset of motor neurons can be visualized in transgenic animals expressing the worm homolog of the synaptic vesicle protein synaptobrevin SNB-1 fused at its C terminus to GFP (Jorgensen *et al.* 1995). The "wild-type" synaptic marker strain was MT8247 *lin-15(n765ts) nIs52*[*Punc-25*::*SNB-1*::*GFP]*; *lin-15 (+)*] *X*. EG1956 *vha-12(n2915sd) nIs52 lin-15(n765ts)* X was the "*vha-12*" synaptic marker strain.

Axon commissure reporter strains: The *unc-47* promoter drives GFP expression in GABA neurons (McIntire *et al.* 1997). Axon branching was analyzed by expressing cytoplasmic GFP in the GABA neurons, using the *unc-47* promoter in the wild-type strain, EG1306 *lin-15(n765ts) oxIs12*[*Punc-47*::*GFP*; *lin-15(+)*] *X*, and the *vha-12* strain, EG1961 *vha-12(n2915sd) lin-15(n765ts) oxIs12 X*.

pHluorin strains: Vesicle pH reporter constructs were constructed similarly to the synaptic marker reporter except GFP was substituted with the pH-sensitive version of GFP, superecliptic pHluorin (Miesenböck *et al.* 1998; Sankaranarayanan *et al.* 2000). The X-ray–integrated line was outcrossed five times to wild-type N2 animals to produce the wild-type pHluorin strain EG3440 *oxIs155* [*Punc-25*::*snb-1*::*superecliptic pHluorin*; *lin-15(+)*] *IV*; *lin-15(n765ts) X*. EG3478 *oxIs155* IV; *vha-12(n2915sd) lin-15(n765ts) X* was the *vha-12* pHluorin strain.

Cell death strains: The caspase-defective strain was EG6313 *ced-3(n717) IV; lon-2(e678) let-44(mg41) X; mnDp31*.

Molecular biology

Sequencing: Sequencing templates were prepared from the PCR-amplified *vha-12* gene from whole worm lysates. To prepare the lysates a single adult hermaphrodite or 5–10 embryos were added to 7.5 μl of distilled water in a thin-walled PCR tube. Two microliters of 5× GC Phusion PCR buffer (Thermo Fisher Scientific) and 0.5 μl of 20 mg/ml proteinase K (New England Biolabs, Ipswich, MA) were incubated at 65° for 1 hr and at 95° for 30 min. PCR was performed with high-fidelity polymerase (Phusion; Thermo Fisher Scientific). PCR products were gel purified (Zymo Research, Irvine, CA) and cloned into a vector and sequenced. To collect *vha-12(mg41)* embryos lacking the free duplication (*mnDp31*), a cohort of 20 embryos laid by *vha-12(n2915)/lon-2(e678) vha-12(mg41)* parents were transferred to a fresh plate. Embryos that did not hatch overnight were collected for *vha-12(mg41)* sequencing.

Minimal rescuing fragment: *vha-12(+)* was generated using the DNA polymerase cocktail Expand (Roche), wild-type genomic DNA, and oligonucleotides oRW025 and oRW026. The PCR product was purified by gel extraction (QIAGEN, Valencia, CA) before injection.

Transcriptional reporter construct: *Pvha-12*::*NLS*::*GFP* was generated by subcloning the PCR product amplified with oligonucleotides oRW075 and oRW077 into pPD95-67 (http://www.addgene.org/Fire_Lab); thus 3 kb of sequence upstream of the *vha-12* start codon was placed 5′ to the nuclear signal sequence contained in pPD95-67.

pHluorin construct: Superecliptic pHluorin is a pH-sensitive version of the green fluorescent protein; at low pH the fluorescence of ecliptic versions of pHluorin is quenched (Miesenböck *et al.* 1998). Superecliptic contains additional mutations that shift the pKa from 7.07 to 7.18 and was described by Sankaranarayanan *et al.* (2000). Superecliptic pHluorin was amplified using *Pfu* DNA polymerase and oligonucleotides oRW109 and oRW110 and subcloned into plasmid pJL35 (*Punc-47*::*SNB-1:GFP*) to make the *Punc-47*::*SNB-1*::*superecliptic pHluorin* plasmid.

Oligonucleotide sequences: Oligonucleotide sequences are as follows: oRW25, ccatttccctgatattgtttctacc; oRW26, gagatatgct gaaaatagctagtgg; oRW075, ggatcctgatattgtttctacc; oRW077, gagctcattcctgaaaaattgc; oRW109, ccggtacccatgagtaaaggagaag; and oRW110, gaattcttatttgtatagttcatcc. To generate overlapping *vha-12* genomic coding sequence fragments, the following oligonucleotides were used: oGE12 cgtatctatcaatgtatctgccac and oGE16 catgacgtcgatagcggagattc, oGE13 gaatggctgccgtt gacgtc and oGE18 ctcgtagatggtggccaaatc, oGE15 gaatctccgc tatcgacgtcatg and oGE20 cacgtgggaagatacggagaag, and oGE17 gatttggccaccatctacgag and oGE22 gttggatttccagctatcac.

Body bending

Body-bending (thrashing) measurements were performed as described by Miller *et al.* (1996). All animals were assayed as 1-day-old adults and body-bending events were captured with video imaging. Individuals were placed into a well of a 96-well tissue-culture plate containing M9 liquid media. After an initial 2-min period, thrashing animals were imaged for 3 min. Images were acquired on an M2 Bio stereomicroscope (Kramer Scientific, Amesbury, MA) equipped with a Pulnix TM-200 CCD camera (Takex). Analog video was digitized using real time (Canopus ADVC 100) and saved to a hard drive as an uncompressed Quicktime video file (Apple). To allow accurate scoring of body bends the image sequence was manually advanced offline in Quicktime Player to count the number of midbody bends.

Aldicarb assays

Aldicarb dose responses were measured for each genotype. Aldicarb dilutions were prepared in S buffer (Sulston and Brenner 1974) and added to pre-weighed, nematode growth

medium plates seeded with OP50 bacterial food. Aldicarb was added to the plates to give final concentrations spanning from 0.1 to 1.3 mM. Twenty to 30 1-day-old adult animals were placed on each assay plate. Paralysis—no locomotion even when prodded by a platinum wire probe—was scored by visual inspection 6–8 hr later, and the fraction of paralyzed animals at each aldicarb dose was recorded. The genotype of the animals was masked to the observer during the paralysis scoring.

Levamisole assays

Levamisole (Sigma, St. Louis) dose responses were measured for each genotype. Levamisole, an acetylcholine receptor agonist, was dissolved in S buffer (Sulston and Brenner 1974) and added to nematode growth medium plates to give final concentrations spanning from 0.01 to 3 mM. Twenty animals were placed on each dose of levamisole, and animals were scored for paralysis 2 hr later. Genotypes were masked to the experimenter at the time the animals were scored.

Body-length measurements

For body-length measurements, stationary individuals on an agar plate seeded with OP50 bacteria were photographed on a stereomicroscope. Images were captured on a Pulnix (Takex) TM-200 CCD camera and digitized (Canopus ADVC 100) to a Macintosh computer. An ImageJ vector line tool was used to make body length measurements head to tail through the midbody. Images were calibrated using a stage micrometer.

Imaging anesthetized adult animals

Fluorescence images were collected on a Zeiss (Thornwood, NY) LSM 5 PASCAL confocal Axioskop FS2 upright microscope. Whole adult animals were mounted on a 2% agarose pad prepared in physiological saline (in mM 150 NaCl, 5 KCl, 1 $MgCl_2$, 1 $CaCl_2$, 10 glucose, 15 HEPES; pH 7.35 adjusted with NaOH and 340 mOsm adjusted with sucrose). Animals were washed from petri plates and transferred to the agar pads on moist filter paper as described in Ramot *et al.* 2008. A 6-μl drop of 1–2% 1-phenoxy 2-propanol was added to straighten animals, and a coverglass was placed on top. To prevent dehydration of the specimens, the edges of the coverglass were sealed with melted petrolatum. Paralyzed animals that rolled ventral-side up (as determined by viewing the vulva location with DIC optics) were imaged. Confocal settings (gain, offset, percentage of power, scan speed, zoom, and pinhole diameter) were identical for quantitative comparison. Genotypes were masked during the acquisition and scoring of synaptic morphology and marker intensity.

Mosaic analysis

To isolate *vha-12* germline mosaics, 724 L4-stage hermaphrodites of the EG7188 strain *vha-12(mg41) lon-2(e678)*; *oxEx1703[vha-12(+)*; *Peft-3*::*GFP*::*HIS-58 (histone H2B)*; *Punc-122*::*GFP coelomocyte marker]* were cultured individually and screened beginning on day 1 of adulthood for an absence of *gfp(+)* embryos. Fourteen putative germline mosaics were isolated that produced broods exclusively of inviable embryos that arrested prior to approximately the 40-cell stage. Of a total of 560 embryos analyzed from the putative germline mosaics, all died as early embryos and exhibited a phenotype distinct from that of *vha-12(mg41)* homozygous embryos produced from *oxEx1703*- or *mnDp31*-transmitting parents or *vha-12(mg41)/+* heterozygotes. Because the *Peft-3*::*GFP*::*histone* transgene is not expressed in the germ line or very early embryos, the conclusion that these 14 animals are indeed germline mosaics is based on the following line of reasoning. Transgenic extrachromosomal arrays are mitotically unstable, frequently being lost at rates of ~1/50–1/200 per cell division (Yochem *et al.* 1998; Yochem and Herman 2003). Were these 14 animals not germline-loss mosaics, then there should have been a distinct class of animals that produce broods of embryos that arrest late in embryogenesis, which was not observed. To test the possibility that the 14 animals had suffered somatic losses that somehow interfered with the production of viable progeny, the animals were analyzed by fluorescent microscopy. All somatic tissues were observed to be *gfp(+)*; thus it was concluded that the 14 animals were likely P4-loss mosaics. Twelve of the mosaics were mated individually to at least 10 wild-type males, but no viable or *gfp(+)* progeny were detected. On the basis of these observations, it was concluded that *vha-12(+)* is both maternally required and sufficient for early embryogenesis, although the exact basis for the lethality will require further investigation.

Analyzing synaptic varicosities in vivo

For analysis of synapses, the synaptic varicosities in the ventral cord motor neurons were imaged. Maximum pixel intensity projections were generated from raw *z*-stacks, and the resulting projected images were analyzed in ImageJ by identifying peaks (>5× baseline). The spacing of synaptic varicosities was measured from peak-to-peak distances. To measure puncta intensity, a square box greater than the size of the average puncta (8 × 8 pixels) was placed around the puncta to determine its optical center of mass (Sankaranarayanan *et al.* 2000). A 4 × 4 pixel box was then placed about this center of mass to measure its mean pixel intensity.

Four-dimensional imaging of embryonic development

Under a standard *C. elegans* dissecting microscope, two- to four-cell stage embryos were collected by cutting open gravid adults in a shallow watch crystal. The embryos were transferred by mouth pipette to a 4% agarose pad. A no. 1.5 coverglass was gently placed over the mounted embryos, a drop of distilled water was drawn across the pad–glass sandwich, and the edges were sealed with melted Vaseline.

Differential interference contrast, time-lapse recordings of embryonic development were recorded on a Zeiss LSM 5

PASCAL confocal microscope equipped with a 63×, 1.4 N.A. plan-apochromat objective. Laser light served as the transmitted light source (488 nm at its lowest power setting). Images were captured on the photomultiplier tube. A stack of 40 images up to 512 × 512 pixels was collected in 0.5-μm increments along the *z*-axis. *Z*-stacks were generated in 5-min intervals for 12–16 hr. The scan speed was set to its fastest possible speed; it took ~1 min to scan one stack. This fast scan speed and minimal laser power setting were not phototoxic as determined by measuring the timing of developmental milestones (comma, 1.5-fold, 2-fold, and 3-fold stage) of wild-type embryos.

Ten apoptotic cells, cell corpses, were tracked in each embryo. A cell corpse was identified as a raised disc-like cell ~2 μm in diameter. To measure cell corpse duration, the image stack was manually inspected to spot the first appearance of a corpse and the first interval in which the corpse disappeared from view. In each time interval the image stack was manually advanced along the *z*-axis to track the corpse in all focal planes. *vha-12(mg41)* embryos lacking the rescuing free duplication were identified from a set of four to five embryos as the embryos that failed to complete embryonic development during the imaging period.

To image the onset of GFP expression from the *vha-12* promoter in embryos, embryos containing the reporter transgene were prepared and imaged in the same manner as described above. The only difference was that the green fluorescence was collected on a separate channel and photomultiplier tube that was equipped with a 505- to 600-nm emission filter.

Electron microscopy

Embryos in a comma stage that do not carry the rescuing array were isolated on the basis of the absence of fluorescence. The embryos were then frozen in a similar manner to that previously described (Rostaing *et al.* 2004; McDonald *et al.* 2010). In short, a type B specimen carrier for a Baltec high-pressure freezer was coated with hexadecence and mounted onto a specimen holder with the flat side facing up. A single-slot TEM grid was placed on top of the specimen carrier. Embryos along with bacteria were scooped using a paintbrush (no. 00) and gently placed in the slot of a grid. The specimen was then capped with another type B specimen carrier with the flat side facing the specimen. The specimen was then frozen and transferred into a cryovial containing 1% osmium and 1% glutaraldehyde in anhydrous acetone. Freeze substitution was carried out in a Leica AFS 2 with the following program: 10 hr at −90°, 5°/hr to −20°, 16 hr at −20°, and 5°/hr to room temperature. When the program ended, the fixatives were washed off with anhydrous acetone six times with each wash, separated by 15 min. The specimens were then infiltrated with Epon-Araldite in a stepwise fashion: 30% for 5 hr, 70% for 6 hr, 90% for overnight, and 100% for 6 hr. Finally, plastic polymerization was carried out in a 60° oven for 48 hr. Sections (50 nm thick) were cut using a Leica UC 6, and 1000 contiguous sections were collected onto formvar-coated grids. These sections were imaged using a Hitachi H7100 transmission electron microscope equipped with a GATAN Orius SC1000 camera.

Results

Viable and lethal mutations in the B subunit of the V-ATPase V1 sector

Mutants with defects in acetylcholine neurotransmission in *C. elegans* exhibit jerky uncoordinated locomotion (Brenner 1974; Miller *et al.* 1996). In a genetic screen for mutants with jerky locomotion we isolated a mutation, *n2915*, that mapped to a narrow interval on chromosome X between *lin-18* and *dpy-23* near the previously uncharacterized *let-44 (mg41)* mutation (Figure 1). *let-44(mg41)* was isolated in an independent screen for recessive X-linked embryonic lethal mutations. The *mg41* mutation failed to complement the locomotion defect of the *n2915* mutation as well as other phenotypes associated with *n2915* mutants (see below). The gene mutated in these strains was identified by DNA microinjection rescue. Nine cosmid clones span the interval between *lin-18* and *dpy-23*. Injection of a single cosmid, C04E10, into *n2915* animals generated three independent lines carrying stable extrachromosomal arrays; two of these three lines rescued the *vha-12(n2915)* uncoordinated phenotype. Cosmid C04E10 was predicted to contain 10 genes (Figure 1). Microinjection of a 5-kb PCR fragment containing the predicted gene F20B6.2 was sufficient to rescue both the uncoordinated phenotype of *n2915* (one of three lines) and the lethality associated with *mg41* (two of three lines). Analysis of the cDNAs from F20B6.2 identified a single reading frame and confirmed the predicted splice pattern (Figure 1). *vha-12* (***v**acuolar **H**$^+$-**ATPase-12***) transcripts encode a 491-amino-acid protein that shares a high level of sequence identity (71–84%) with other V-ATPase B-subunit genes (Supporting Information, Figure S1). The *C. elegans* genome contains a second locus, called *spe-5* (Y110A7A.12), that encodes a V-ATPase B subunit. Because *spe-5* mutants are defective for spermatogenesis (see accompanying article by Gleason *et al.* 2012) and *vha-12* null mutants are lethal, these loci are not fully redundant and independent functions can be characterized.

Sequencing the *vha-12* locus from the *n2915* and *mg41* mutants identified the nucleotide changes associated with these mutations and confirmed the identity of *vha-12* (Figure S1). *vha-12(n2915)* is a C to T transition in the third exon of F20B6.2 that results in the substitution of a highly conserved alanine at position 385 with a valine in the predicted protein (Figure S1). This allele is an antimorphic allele by genetic criteria, since it is semidominant and reduces V-ATPase function (see below). We generated a molecular model of VHA-12 by threading its sequence onto the crystal structure of the related archaebacteria *Methanosarcina* A_1 B subunit (Figure S2). The *vha-12(n2915)* mutation is near the catalytic site of the ATPase and in a region

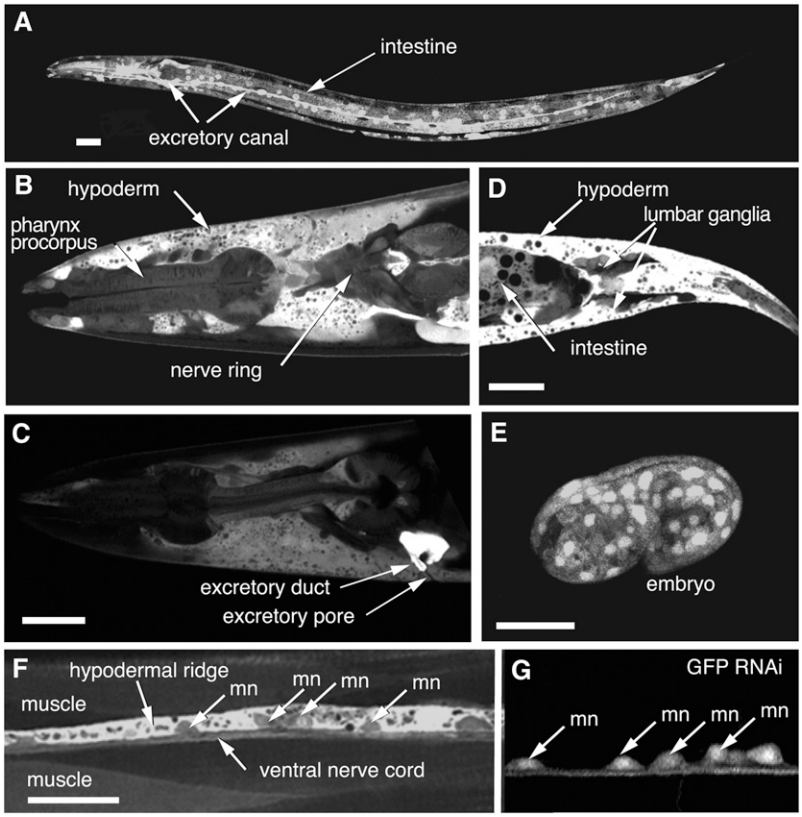

Figure 2 *vha-12* is expressed broadly in somatic tissues. GFP expression is driven by the wild-type *vha-12* promoter. Three kilobases of DNA upstream of the *vha-12* translation initiation codon were fused in frame to GFP (strain EG2410). (A) Image of an L3 larva showing strong *vha-12* promoter activity in the excretory cell and the intestine. (B) Confocal section of an adult head showing *vha-12* promoter activity in pharynx, neurons, and hypoderm. (C) Confocal section of adult head showing intense *vha-12* expression in excretory duct. (D) Confocal section of an adult tail showing expression of neurons in the tail ganglia and tail hypodermis. Plane of section is coronal. (E) Most, if not all, cells in the comma-stage embryo show strong *vha-12* promoter activity. (F) Ventral hypoderm, muscle, and motor neurons (mn) of the ventral nerve cord. (G) The nervous system expresses *vha-12*. The transgenic strain was fed GFP dsRNA to eliminate expression in nonneuronal tissue; the nervous system is insensitive to RNA interference.

associated with a human kidney disease mutation (Figure S1). Alanine 385 is juxtaposed to a conserved glutamate (Glu149), a residue that is polymorphic, and possibly dysfunctional, in humans (human B1 Glu161Lys); B1 subunit proteins containing the Lys161 polymorphism are made but do not function in heterologous assays (Figure S2) (Fuster *et al.* 2008). Alanine 385 is five residues downstream from a conserved and essential arginine residue (Arg380) (Liu *et al.* 1996; Nishi and Forgac 2002). In the crystal structure of the related F-ATPase subunit α, this arginine (Arg373) rests in the catalytic pocket of the ATPase domain where it stabilizes the terminal phosphate group during ATP hydrolysis (Abrahams *et al.* 1994). Mutation of the arginine abolishes V-ATPase function in yeast, and the homologous residue in the human B1 subunit is linked to distal tubule renal acidosis (Liu *et al.* 1996; Vargas-Poussou *et al.* 2006). Given the propinquity of Ala385 to Arg380, it is likely that the *n2915* lesion impairs ATP catalysis.

Sequence analysis of *vha-12(mg41)* arrested embryos identified two mutations within the gene: a C to T transition at nucleotide 506 and a C to A transversion at nucleotide 698. The latter mutation results in a missense mutation changing the nonconserved arginine 200 into a serine. The upstream mutation results in an amber stop at amino acid position 153, thereby truncating 70% of the protein (Figure S1). Genetic criteria indicate that this mutation is a null allele. First, *mg41* is recessive: *vha-12(mg41)* heterozygotes are indistinguishable from the wild type. Second, *mg41* behaves as a null in regard to the weaker allele: *vha-12 (n2915)/vha-12(mg41)* animals exhibit a more severe phenotype than *vha-12(n2915)* homozygotes (Figure S3). Subunit B is a major constituent of V_1 sectors of the V-ATPase and is required for full V_1 sector assembly (Kane 2006). Because this nonsense mutation would delete important interface residues, it is likely that *mg41* abolishes V_1 complex assembly and represents a complete loss of V_1 functions. Thus, the *n2915* and *mg41* alleles provide reagents capable of characterizing the role of acidic organelles during development as well as in adult tissues in *C. elegans*.

vha-12 is widely expressed in somatic cells

Different V-ATPase subunit isoforms may be expressed in different subsets of tissues. To test whether *vha-12* is expressed in a specific cell type, we generated a transcriptional reporter in which the expression of GFP fused to a nuclear localization tag (SV40) was placed under the control of the *vha-12* promoter: 3 kb of DNA sequence preceding the predicted ATG start codon (Figure 2). This reporter construct was introduced via microinjection into the gonad to generate the stable extrachromosomal array, *oxEx192*. *vha-12* is broadly expressed in most, if not all, somatic cell types in larvae and adults (Figure 2A). Robust GFP expression is observed in the H-shaped excretory cell, the excretory pore, the intestine, and hypodermal cells (Figure 2, B–F). GFP reporter expression is observed at low levels in muscle. Consistent with the uncoordinated phenotype, expression is observed in all neurons (Figure 2G).

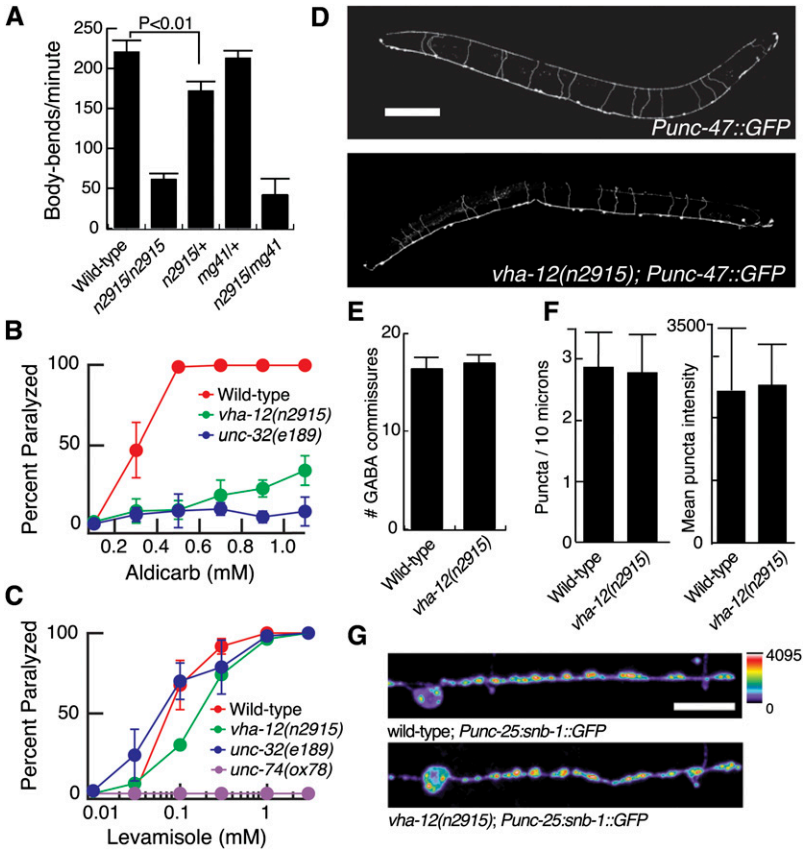

Figure 3 Neuronal function is impaired in *vha-12(n2915)* mutants. *vha-12(n2915)* animals are uncoordinated. (A) Thrashing. *vha-12(n2915)* body-bending rate in liquid media was severely reduced compared to that of wild-type animals and the *mg41* mutation failed to complement the bending defect. The bending rate of *vha-12(n2915)* heterozygotes was less than that of wild type but greater than that of *vha-12(n2915)* homozygotes. (B) Aldicarb sensitivity. *vha-12(n2915)* mutants were strongly resistant to the paralyzing effects of aldicarb. (C) Levamisole sensitivity. Homozygous *vha-12(n2915)* mutants were slightly resistant to the paralyzing effects of the postsynaptic acetylcholine receptor agonist levamisole. Values are mean ± SEM of five independent experiments; *unc-32(e189)* is a neuronal mutation in the *a* subunit of the V_o domain of the V-ATPase (Pujol *et al.* 2001). (D) GABA motor neuron axonal morphology is not perturbed. Images show animals expressing GFP driven by the GABA-specific *unc-47* promoter in wild type (*oxIs12*). Bar: 0.1 mm. (E) No significant difference in axon number from GABA neurons was detected between wild-type and *vha-12(n2915)* animals ($n = 3$). (F) Left, the spacing of synaptic puncta was approximately three puncta per 10 μm in wild-type and *vha-12(n2915)* animals (2.87 ± 0.58, $n = 8$ wild-type animals, and 2.79 ± 0.62, $n = 9$ *vha-12(n2915)* animals, mean ± SD). Right, quantification of intensity of synaptobrevin-GFP staining puncta. These puncta represent synaptic varicosities. (G) *vha-12(n2915)* synaptic morphology was normal and expressed normal quantities of the synaptic vesicle (synaptobrevin) GFP fusion protein. Bar: 10 μm.

Neurotransmission is disrupted in vha-12 (n2915) mutants

The locomotory defect in the *vha-12(n2915)* mutants suggests a neuromuscular defect. Locomotion can be quantified by counting the number of body bends of an animal placed in a drop of liquid medium for a brief period (Miller *et al.* 1996). Wild-type animals swim rapidly in liquid (221 ± 14 bends per minute, $n = 3$), whereas homozygous *vha-12 (n2915)* animals swim slowly (62 ± 7 bends per minute, $n = 3$, $P < 0.0001$) (Figure 3A). Compared to the wild type, heterozygous *vha-12(n2915)* animals had a statistically significant reduced swimming rate (172 ± 11 bends per minute, $n = 3$; $P < 0.01$, two-tailed *t*-test) and thus *n2915* is a semidominant mutation. To determine whether the neuromuscular defect was presynaptic, we measured the sensitivity of *vha-12(n2915)* mutant animals to drugs that affect neurotransmission. Acetylcholinesterase degrades acetylcholine after it has been released from neurons. The drug aldicarb inhibits acetylcholinesterase and the accumulation of acetylcholine causes animals to hypercontract; whereas animals with defects in acetylcholine release are resistant to aldicarb (Miller *et al.* 1996). When wild-type animals were exposed to 0.7 mM aldicarb, 100% were paralyzed after 2 hr (Figure 3B). However, only 18% of *vha-12 (n2915)* animals (±9%, $n = 5$ assays) were paralyzed after a 2-hr exposure to aldicarb. As a reference we analyzed aldicarb sensitivity of another strain defective in a V-ATPase subunit. The *unc-32(e189)* mutation truncates a neural-specific isoform of the V_o subunit a (Pujol *et al.* 2001). Like *vha-12(n2915)* mutant animals, *unc-32(e189)* animals are viable as adults but uncoordinated. *unc-32(e189)* mutants were also significantly aldicarb resistant with only 8.5% (±9%, $n = 5$ assays) paralyzed after 2 hr exposure. The aldicarb resistance of the *vha-12(n2915)* mutant animals suggests a role for the V-ATPase in neurotransmission.

Aldicarb resistance can be explained by either a decrease in acetylcholine release or decreased sensitivity of the muscle to acetylcholine. Muscle sensitivity can be determined by measuring the fraction of animals paralyzed by the acetylcholine receptor agonist levamisole. The sensitivity of *vha-12(n2915)* to the postsynaptic acetylcholine receptor agonist, levamisole, was not detectably different from that in wild-type animals (Figure 3C). One hundred percent of wild-type animals were paralyzed by 1 mM levamisole, and 96% of *vha-12(n2915)* mutants were paralyzed by the same dose (±4%, $n = 5$; $P = 0.35$). The V_o mutant *unc-32(e189)* also *exhibited* comparable sensitivity to levamisole to that of wild-type animals. Taking the aldicarb resistance and levamisole sensitivity together, these pharmacological assays suggest *vha-12(n2915)* mutant animals have a defect in neurotransmitter release.

We examined whether there were neuronal developmental defects in *vha-12(n2915)* mutants by imaging axonal morphology and synaptic formation. No significant difference in

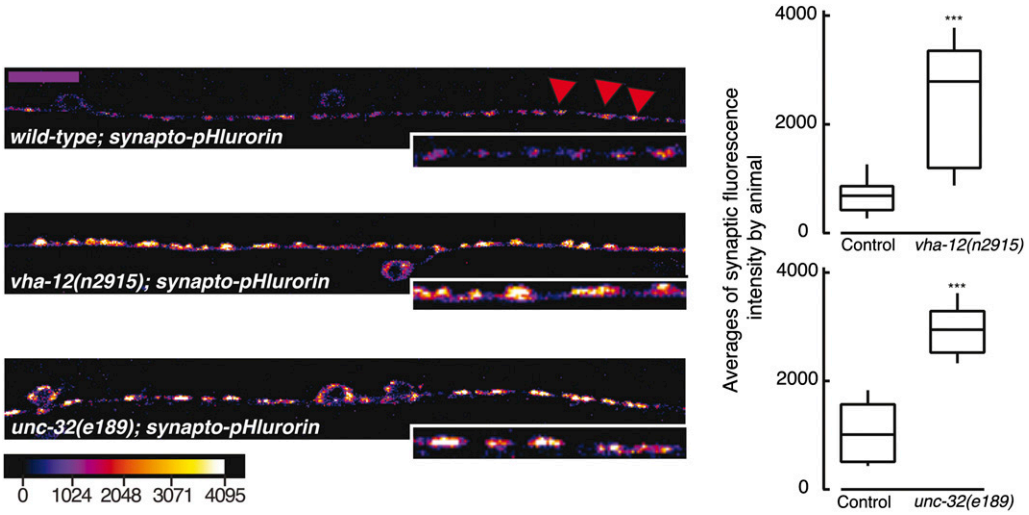

Figure 4 Synaptic vesicle acidification is defective in V-ATPase mutants. Images show the ventral nerve cord of adult hermaphrodites expressing the pH-sensitive GFP reporter (pHlourin) targeted to the lumenal domain of synaptobrevin. Fluorescence from pHluorin-tagged synaptic vesicles is increased at both V_1 and V_o V-ATPase mutant synaptic varicosities (for example, red arrowheads). Top, wild-type ventral cord motor neuron; middle, V_1 sector mutant *vha-12(n2915)* motor neuron; bottom, V_o sector mutant *unc-32(e189)* motor neuron. Box and whisker plots (right) show the average synaptic fluorescence from individual animals, comparing V-ATPase mutant synaptic puncta to matched wild-type controls. Synaptic *vha-12(n2915)* puncta were compared to the wild type [average 665 ± 210 fluorescence units, $n = 10$ for wild type; 2494 ± 334 fluorescence units, $n = 10$ for *vha-12(n2915)*, $P < 0.0001$, two-tailed *t*-test]. Fluorescence at synaptic puncta in *unc-32(e189)* mutants was increased relative to a separate set of wild-type animals imaged in parallel [average 1060 ± 155 fluorescence units, $n = 12$ for wild type, 2939 ± 123 fluorescence units, $n = 13$ for *unc-32(e189)*, $P < 0.0001$, two-tailed *t*-test]. Median is the middle line and boxes define the 25th and 75th percentiles. The top and bottom ends of the box whiskers are the 90th and 10th percentiles, respectively. Increased fluorescence intensity is consistent with more alkaline vesicles. Bar: 10 μm. Insets are 2× magnified regions of interest.

the number of GABA commissures was found between wild-type and *vha-12(n2915)* animals (Figure 3, D and E; wild type, 16.4 ± 1.1, $n = 7$; *vha-12(n2915)*, 17.0 ± 0.8, $n = 7$, $P = 0.3$, unpaired *t*-test). The distribution and expression levels of a transgenic synapse marker in ventral GABA motor neurons was also not significantly altered in *vha-12(n2915)* mutants (2.87 ± 0.58 varicosities per 10 μm, $n = 8$ in wild type *vs.* 2.79 ± 0.62 varicosities per 10 μm, $n = 9$, $P = 0.8$; Figure 3, F and G). The normal distribution of synapses and axon morphology suggest that neuronal development in *vha-12(n2915)* mutants is not severely impaired.

We expected that synaptic vesicles would not be acidified in the V_1 mutant, since neurotransmitter loading into vesicles relies on exchange of protons for neurotransmitter molecules. We examined whether synaptic vesicles were acidified by tagging the lumenal domain of synaptobrevin with superecliptic pHluorin, a pH-sensitive GFP reporter. Superecliptic pHluorin has the property that at low, acidic pH, its fluorescence is quenched. Superecliptic pHluorin has a reported pKa of 7.1 and is therefore particularly sensitive in a physiological pH range (Miesenböck *et al.* 1998; Sankaranarayanan *et al.* 2000). pHlourin puncta were on average threefold brighter in *vha-12(n2915)* mutants compared to the wild type (Figure 4). Similar results were seen in the V_o subunit *a* mutant *unc-32(e189)*. Since the pH reporter was associated with the lumenal domain of a synaptic vesicle protein, if the protein is on the plasma membrane, the pH reporter will be exposed to the extracellular environment and would fluoresce more brightly. However, since synaptobrevin labeled with a non-pH–sensitive GFP vesicle reporter was punctate rather than diffuse, it is unlikely that synaptobrevin resides on the surface due to a defect in endocytosis. The simplest interpretation of the increased vesicular pHluorin fluorescence is that *vha-12(n2915)* mutant vesicles are less acidic than the wild type.

Epidermal functions of V_1

In addition to a semidominant uncoordinated phenotype, *vha-12(n2915)* mutants exhibit a dominant dumpy phenotype that can be quantified as a reduced body length (Figure 5). Oddly, the shortened body-length phenotype was detected in heterozygotes but not in homozygotes. A dumpy phenotype was detected when the *n2915* allele was heterozygous with either the wild-type or the *mg41* allele (Figure 5). It was possible that the dominant dumpy phenotype could be caused by a linked mutation; however extensive outcrossing was unable to separate the uncoordinated and dumpy phenotypes, and the dumpy phenotype is fully rescued by the *vha-12* transgene (*oxEx552* in strain EG3250; Figure 5, column 3). The dumpy phenotype is often associated with defects in cuticle formation caused by impaired function of underlying epidermal cells (McMahon *et al.* 2003; Page and Johnstone 2007) and is consistent with the expression of the *vha-12* reporter in epidermal cells. Another epidermal defect was the high incidence of 1-day-old adult *vha-12(n2915)* heterozygotes dragging recently molted cuticle [11/40 of *n2915/+ vs.* 0/20 of wild-type and 0/33 of *vha-12(n2915)* homozygotes, Figure S4]. Interestingly, reduced body length is also observed in specific *vha-5* mutants that preferentially disrupt cuticle formation (Liégeois *et al.* 2006); *vha-5* encodes a *C. elegans* V_o *a* V-ATPase subunit homolog expressed in the epidermis. These results suggest that epidermal function is not limited to V_o-specific roles, but may instead require the full activity of a V_1V_o–H^+-ATPase complex.

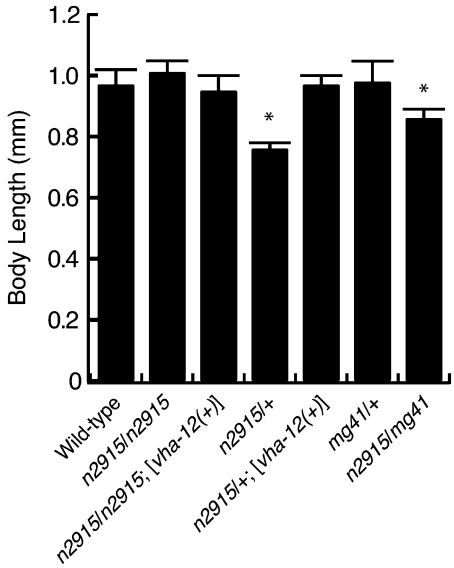

Figure 5 Reduced body length in *vha-12(n2915)* heterozygotes. Animals heterozygous for the *vha-12(n2915)* mutation were shorter than wild-type animals [wild type (WT), 0.97 ± 0.05 mm, $n = 5$; *vha-12(n2915)/+*, 0.76 ± 0.02 mm, $n = 5$; $P < 0.0001$, two-tailed *t*-test *vs.* WT; and *n2915/mg41*, 0.81 ± 0.07 mm, $n = 9$; $P = 0.001$ *vs.* WT). All animals were scored as 1-day-old adults. Asterisks indicate statistically significant different values from wild type.

vha-12 is required maternally for early embryonic development, not oogenesis

Our transcriptional reporter did not indicate expression of *vha-12* in the germ line of adults. However, extrachromosomal arrays are usually silenced in the germ line and lack of expression from a fluorescence reporter construct is not conclusive. In fact, *vha-12* is expressed during oogenesis on the basis of SAGE analysis (Wang *et al.* 2009) and transcripts are observed in early embryos by *in situ* hybridization (Figure S5; Shin-i and Kohara 2005).

Mosaic analysis further demonstrates that expression of *vha-12* in the adult germ line is required for proper development of embryos soon after fertilization. We rescued *vha-12(mg41)* mutants with a *vha-12(+)* extrachromosomal array containing a GFP marker (see *Materials and Methods*). We then screened for loss of the extrachromosomal array in the progenitor germ cells. From 724 hermaphrodites, 14 germline-loss mosaics were recovered. Gonad and oocyte morphology was normal in mosaics that seem to have lost the rescuing copy of *vha-12* in the P4 precursor cell to all germ cells (Figure 6A). Moreover, fertilized embryos were observed in the uterus, indicating that oocyte and sperm formation is normal in the absence of *vha-12*. These mosaics produce broods composed of only dead embryos (Figure 6B). The maternally mutant embryos arrest prior to the 40-cell stage, typically by the 28-cell stage, whereas zygotic mutants complete cell divisions during embryogenesis (Figure 6E). The maternally mutant embryos are grossly abnormal and there are examples of multinucleated cells (Figure 6B). Interestingly, embryos that fail to release extracellular components from cortical granules exhibit defects in cytokinesis and give rise to similar multinucleated cells (Bembenek *et al.* 2007; Sato *et al.* 2008). To determine whether zygotic expression can rescue the early embryonic lethality, 12 germline mosaics were mated with wild-type males. No rescued progeny were observed in these matings, suggesting that a wild-type copy of the *vha-12* gene from a wild-type sperm cannot provide *vha-12* function. The *vha-12* gene is on the X chromosome and it is known that many genes on the paternal X chromosome are silenced during early embryogenesis (Bean *et al.* 2004). Thus *vha-12(+)* is expressed in the germline and is required for early embryogenesis but not in the formation of germ cells.

vha-12 is required zygotically for morphogenesis

Zygotic expression begins midembryogenesis and appears to be expressed in all cells (Figure 6, C and D). To examine the precise onset of zygotic *vha-12* gene expression, we performed time-lapse microscopy on isolated embryos carrying our transcriptional reporter construct. One- to two-cell stage embryos were prepared for time-lapse confocal imaging, monitoring both DIC for morphology and fluorescence for GFP. Fluorescence was not detected through the first 200 min of development; presumably maternally contributed VHA-12 suffices for development during the rapid cell divisions that mark this stage. At the end of gastrulation, ~200–220 min after the first cell cleavage, fluorescence driven by the *vha-12* promoter first appears in embryos, particularly in cells along the midline. Robust fluorescence from the *vha-12* reporter is observed in comma-stage embryos. Thus, the first stages of *C. elegans* development occur without detectable levels of transcription from the *vha-12* locus.

A requirement for zygotic expression appears during morphogenesis (Figure 6E), soon after transcription from the locus begins. Homozygous *vha-12(mg41)* progeny {*vha-12(m+z−)* from *vha-12(mg41)/+* or *vha-12(mg41)*; *Dp[vha-12(+)]* mothers} were analyzed using time-lapse video microscopy. In these experiments one- to two-cell stage embryos were dissected out of gravid hermaphrodite *mg41/mg41*; *mnDp3* adults, and each embryo was imaged until either it hatched or it arrested. Approximately half of the embryos did not hatch, consistent with the reported loss of the *mnDp31* duplication. Of the embryos that did not hatch, 70% arrested at the 2- to 3-fold stage (450–520 min, 17/25 animals) and 28% of the animals arrested earlier, at the lima bean stage (380 min, 4/25), at the comma stage (395 min, 2/25), or at the 1.5-fold stage (430 min, 1/25). In this assay, one morphologically abnormal embryo (1/25) hatched but arrested development shortly thereafter; these rare escapers are likely due to mosaicism, that is, the presence of the rescuing duplication in some cells. Thus, the first appearance of zygotic *vha-12* gene expression coincides with the period that just precedes the requirement of *vha-12* during morphogenesis.

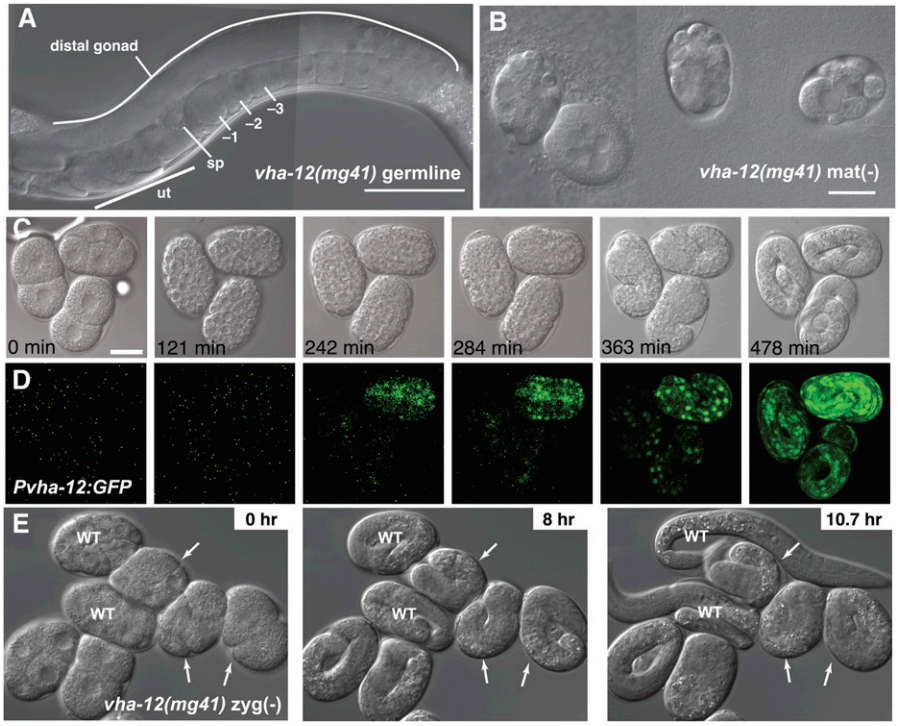

Figure 6 vha-12 is required for embryonic development. (A) Normal somatic and germline morphology is observed in *vha-12(mg41)* mosaics in which the rescuing array was lost in the P4 germline progenitor cell. The distal gonad, uterus (ut), spermatheca, sperm (sp), oocytes (numbered relative to spermatheca, -1,-2,-3), and ovulation are normal. Inviable embryos are located in the uterus. Bar: 50 μm. (B) Loss of maternal *vha-12(+)* expression results in early embryonic arrest. *vha-12(mg41) maternal(−)* embryos were produced from *vha-12(mg41)* germline clones from EG7188 *vha-12(mg41)*; *oxEx1703* hermaphrodites. Multinucleated cells were frequently observed. Animals arrested with <40 cells (560 embryos from germline clones). Bar: 20 μm. (C and D) Expression of GFP driven by the *vha-12* promoter is not detected in early embryos (approximately between 0 and 200 min after the first cell cleavage). Images are from a movie of embryonic development from a *Pvha-12*::*GFP* transgenic strain. In each row a transmitted light image of the embryo, at a single plane (C), is shown along with the projected image acquired from the GFP channel (D). Bar: 20 μm. (E) *vha-12(mg41)* homozygotes arrest between two- and threefold. Three panels from a time-lapse movie were taken in a single focal plane of *vha-12(mg41) lon-2(e678)* embryos (arrows) produced from a *vha-12(mg41) lon-2(e678)*; *mnDp31* hermaphrodite. See also File S6.

An apoptosis defect in strong vha-12 mutants

In the course of our video microscopy analyses of maternally rescued *vha-12(mg41)* homozygous embryos, we observed a striking phenotype in the clearance of apoptotic cells (see movies in File S1, File S2, File S3, File S4, File S5, and File S6). We tracked the persistence of apoptotic cell corpses with four-dimensional video recordings. In the course of normal *C. elegans* hermaphrodite embryogenesis 113 cells undergo programmed cell death (Sulston *et al.* 1983). Using differential interference contrast optics, apoptotic *C. elegans* cells appear as raised disc-like structures ~2 μm in diameter (Conradt and Xue 2005). Cell corpses are normally engulfed by neighboring cells and degraded. In the wild type, most cell corpses (73%, 16/30) were cleared within 20 min of their first appearance, consistent with previous studies (Yu *et al.* 2006), and no corpses persisted >60 min (Figure 7). The average wild-type corpse duration was 18 ± 2 min ($n = 30$). In the wild type, no cell corpses (0/15) remained >60 min. By contrast, average corpse duration was 47 ± 3 min ($n = 56$; $P < 0.0001$ *vs.* wild-type, Mann–Whitney test). In *vha-12(mg41)* embryos 36% of cell corpses (20/56) persisted ≥60 min. To demonstrate that these cell deaths were due to apoptosis and not degenerative or necrotic cell death, we blocked apoptosis using a *ced-3* mutation. CED-3 is the caspase that is required for apoptosis (Ellis and Horvitz 1986; Yuan *et al.* 1993). No cell corpses were observed in a *ced-3 (n717) vha-12(mg41)* double mutant. The life span of *vha-12(mg41)* mutant embryos was not increased by suppressing programmed cell death; the double mutant embryos we observed arrested at the twofold stage.

The delay in clearance of dying cells does not result from a general slowdown of embryonic development. We timed easily observable milestones in *vha-12(mg41)* embryos. The lima bean to comma stage took 48 ± 3 min in wild type and 49 ± 10 min in *vha-12(mg41)* mutants; comma to 1.5-fold took 36 min in wild type and 29 ± 5 min in *vha-12(mg41)*; 1.5-fold to 2-fold took 10 ± 2 min for wild type and 12 ± 0.2 min for *vha-12(mg41)*. In the rare cases where a *vha-12 (mg41)* embryo survived to a 3-fold stage, *vha-12(mg41)* took 75 min to progress from the 2-fold to the 3-fold stage and the wild type took 70 ± 2 min [$n = 3$ wild type and $n = 6$ *vha-12(mg41)*]. On the basis of these developmental timing observations, we conclude that although mutant embryos arrest prior to completing morphogenesis, the rate of morphogenesis leading up to arrest is not slowed down in *vha-12(mg41)* mutants.

The lingering of corpses is also not caused by a defect in cell engulfment by neighboring cells. To determine whether corpses can be engulfed in *vha-12(mg41)* mutants we analyzed comma-stage embryos using electron microscopy. Corpses with visible nuclei and mitochondria were observed inside 3 cells from among the ~60 cells examined (Figure 8A). The corpses were fully enveloped in the two cells that were reconstructed from serial sections, demonstrating that cells were capable of engulfing dying cells. Most cells also exhibited abnormal lysosomes that were filled with dense membranous matter (Figure 8B). Although there

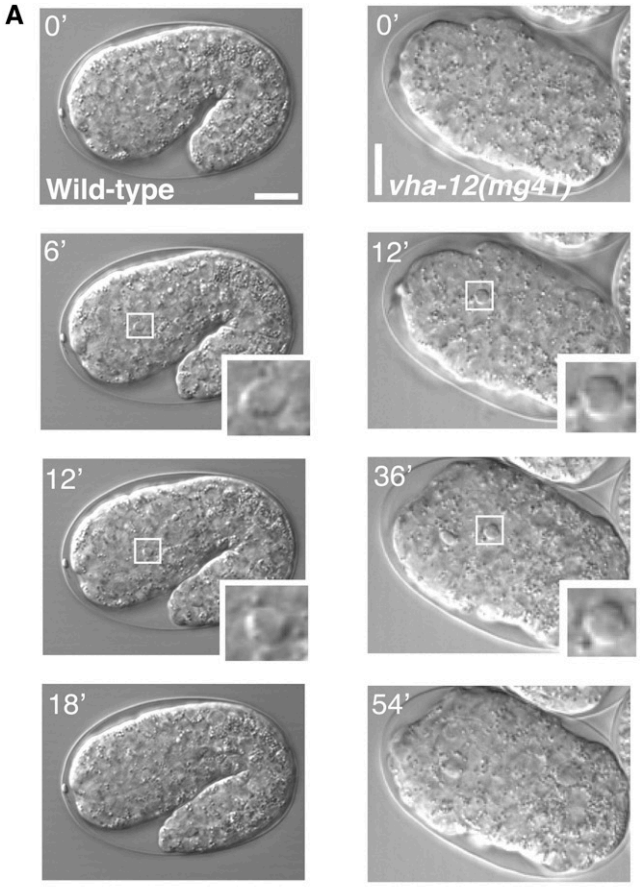

Figure 7 Apoptotic cell corpses persist in *vha-12(mg41)* mutants. (A) Representative images from movies of wild-type and *vha-12(mg41)* embryos. Insets are 2×-scaled images of the apoptotic cell being tracked in each image; the nuclei of dying cells have a characteristic raised button appearance in DIC. Bar: 10 μm. (B) Scatter plot indicating the duration of individual cell corpses; each point represents the duration of a single tracked corpse. Ten apoptotic cell corpses were tracked in three to six embryos. Most wild-type cell corpses are cleared by 20 min. Most *vha-12 (mg41)* cell corpses require >30 min to clear, if at all. Arrows indicate the time at which tracking was stopped. Presumably these corpses persisted longer than shown.

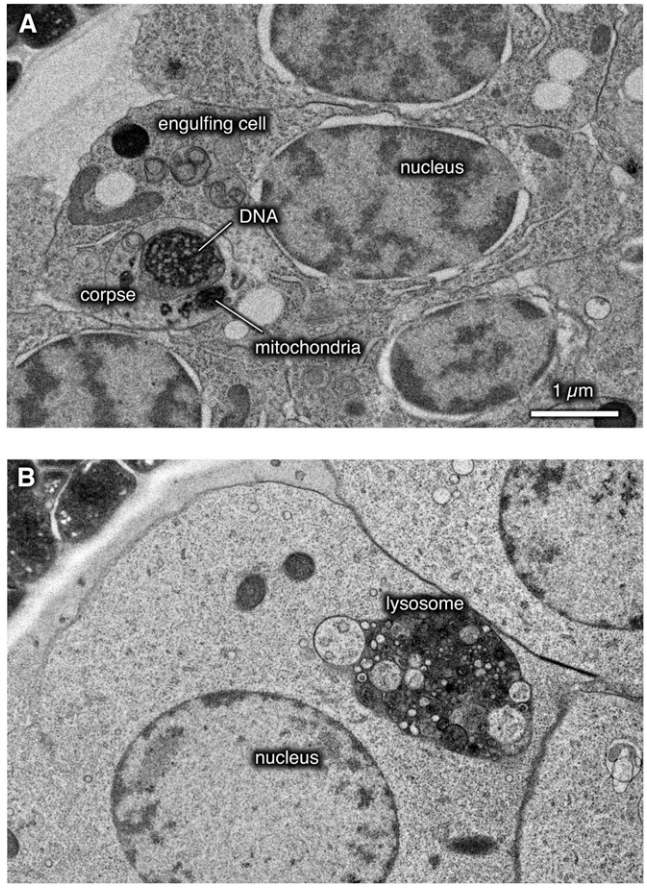

Figure 8 Cell corpses are engulfed in *vha-12(mg41)* mutants. Electron micrographs show cells in comma-stage embryos in *vha-12(mg41)*. *vha-12(mg41)* embryos were recognized as segregants from the rescued strain EG7188 that lacked GFP expression from the *Peft-3:GFP* construct that marked the rescuing array. (A) A cell corpse can be observed in an engulfing cell. A condensed nucleus ("DNA") and mitochondria from the corpse are undegraded and surrounded by the single membrane of a lysosome. Reconstruction of this cell from serial electron micrographs demonstrated that the corpse was completely surrounded by the engulfing cell. (B) Most cells in the *vha-12(mg41)* mutant embryos contained swollen lysosomes that contained many undegraded vesicles.

is not an absolute defect in engulfment, it is possible that corpse clearance is slowed either because the engulfing cell is not fully functional due to the lack of a functional lysosome or because the dying cell cannot undergo programmed cell death properly in the absence of acidified compartments.

Discussion

How important is acidification of organelles and secretion of protons by genetic criteria? By characterizing two mutations in the catalytic B subunit of the V-ATPase, we conclude that the B subunit, and by extension the entire V_1 complex, is required for normal cell proliferation, corpse clearance, morphogenesis, neurotransmission, and molting. In addition, given the high expression of *vha-12* in the excretory canal, it is likely that the V-ATPase is involved in secretion of protons in *C. elegans* as in the kidney of higher organisms. In short, VHA-12 is widely expressed and contributes to a variety of cellular functions. Our results confirm and extend

observations of the role of V-ATPase in development and in the function of adult cells. Two issues bear further discussion: Are there differential functions for the V_o and V_1 sectors? And are there differential functions provided by isoforms of particular subunits within these sectors?

Sector diversity: V_o vs. V_1 functions

The V-ATPase is required to acidify lysosomes and activate degradative enzymes. It is expected that both sectors will be required for acidification since the V_1 sector forms the ATPase catalytic site and the V_o sector forms the pore that translocates protons across the membrane. In addition, it has been proposed that the V_o sector has additional functions independent of the V_1 sector (Peters *et al.* 2001). Specifically, the transmembrane V_o sector may mediate membrane fusion in the vacuole in yeast. To determine whether the V_o sector has additional functions, the phenotypes of V_1 and V_o sector mutations must be compared. If true, the V_o sector mutants would exhibit additional phenotypes not observed in V_1 sector mutants. Unfortunately, mutants lacking V_1 sector functions have not been well characterized.

Here we characterize the phenotype of a null mutation in the B subunit of the V_1 encoded by *vha-12*. First, expression from the *vha-12* gene begins when cell divisions are nearly complete (~5 hr after the first cleavage). Most mutant embryos arrest 3 hr later during morphogenesis as the embryos elongate (two- to threefold stage 8 hr after the first cleavage). During embryogenesis 113 cells undergo programmed cell death (Sulston *et al.* 1983). Normally these dying cells are engulfed by neighboring cells and degraded in the phagocytic pathway (He *et al.* 2009). Specifically three things need to happen for an apoptotic corpse to be cleared: (1) the corpse needs to be engulfed, (2) the resulting phagosome has to fuse to a lysosome, and (3) acid-activated proteases in the lysosomes need to degrade the corpse. V-ATPases in different systems have been proposed to act in facilitating internalized material (Dettmer *et al.* 2006; Hurtado-Lorenzo *et al.* 2006), in organelle fusion steps (Peri and Nüsslein-Volhard 2008; Williamson *et al.* 2010), and in lysosomal degradation competence (J. H. Lee *et al.* 2010). We sought to define at what steps the V-ATPase is involved in *C. elegans* apoptotic corpse clearance. At the light microscopic level corpses in the *vha-12* mutant take much longer to clear than in a wild-type background. Ultrastructural analysis of *vha-12* mutants demonstrated that corpses are engulfed; serial reconstruction of two corpses demonstrated that the cell was completely engulfed by a neighboring cell. Engulfed corpses appeared to progress to a lysosome because the contents of a corpse were surrounded by a single membrane. The corpses had progressed to the lysosome but undegraded nuclei and mitochondria were clearly visible inside the organelle, a phenotype that one might expect in an acidification-defective mutant. Although we were not able to measure acidification of lysosomes in the arrested embyro, we were able to confirm a defect in acidification of synaptic vesicles in the weaker allele, confirming that the V_1 sector is required to pump protons into organelles. Moreover, lysosomes observed in electron micrographs were swollen and filled with membranes in most cells of mutant embryos, suggesting that there are defects in lysosomal functions. These results suggest that a major role of the V-ATPase is to acidify the lysosome.

In two studies, mutations in the conserved *a1* subfamily of V_o *a* subunits caused defects in the progression of phagocytic compartments, suggesting an additional function for the V_o sector. In zebrafish, apoptotic corpses were internalized but accumulated as immature phagosomes that did not fuse with the lysosome in animals where V_o *a1* gene expression was knocked down by morpholinos (Peri and Nüsslein-Volhard 2008). In *Drosophila*, autophagic vesicles accumulated in *vha100-1* mutants (Williamson *et al.* 2010). In both of these studies the authors observed normal acidification of some organelles. These studies suggest that V_o has an acidification-independent function to promote vesicle trafficking and maturation of phagolysosomes. The assumption is that the V_1 sector is still functional and can acidify organelles in these mutants despite mutations in the V_o *a1* isoform. One problem with the studies of V_o sector mutants is that it is not clear whether the phagosome was acidified and not some other compartment and whether acidification was truly normal. Moreover, it is not clear how acidification takes place when the pore-forming *a* subunit expression is knocked down (Peri and Nüsslein-Volhard 2008) or is presumably absent (Williamson *et al.* 2010). One possibility is that there is enough residual function from the *a1* subunit or from another partially redundant *a* subunit. Alternatively, there may be V-ATPase–independent mechanisms for acidification (Orlowski and Grinstein 2007). Nevertheless, with the caveat that we lack kinetic information about phagosome maturation, our data align with the conclusion from these articles: we did not detect a major defect in phago-lysosome maturation because presumably, the V_1 sector is absent in *vha-12* mutants but the fuosgenic V_o sector is present.

On the other hand, another study finds that fully assembled V-ATPases are required for autophagsome maturation *and* lysosomal degradation competence (J. H. Lee *et al.* 2010). If the V_o is not targeted to the lysosome, neither are V_1 subunits. J. H. Lee *et al.* (2010) found that presenilin is required for a post-translational modification of a V_o *a* subunit that targets the subunit to the lysosome. In the absence of presenilin, autophagosomes accumulate, and of those autophagosomes that do fuse to lysosomes, autophagoctyosed material was not degraded. It must be emphasized that we observe a similar phenotype with the loss of the V_1 sector in *vha-12(mg41)* mutants. Together these data suggest that loss of either the V_o or the V_1 sector results in the same phenotype, probably due to a defect in acidification as well as a defect in maturation. We are left with contradictory conclusions. In hindsight, there are two problems in these studies. First, it is not clear whether the *a* subunit

mutants represent a complete loss of V_o sector function, given that there are multiple isoforms of *a* subunits in all eukaryotic genomes analyzed. Second, the comparisons described above are between mutants in different organisms. In the future studies must be performed comparing V-ATPase V_1 and V_o sector mutants in the same organism in which direct measurements of organelle pH are made with measures of organelle fusion in parallel.

V_1 diversity: VHA-12 vs. SPE-5

Why do organisms encode a diversity of individual subunits for the V-ATPase in their genomes? The V_o sector subunit *a* in particular shows a large amount of diversity. For example, in *C. elegans* there are four genes encoding the *a* subunit with multiple alternative splice forms (Figure 1A) (Oka *et al.* 2001; Pujol *et al.* 2001; S. K. Lee *et al.* 2010). Mammals also encode four *a* subunits and yeast encode two *a* subunits (Toei *et al.* 2010). V_1 sector subunits can also be diverse; for example mammals encode two V_1 B subunits, two C subunits, two E subunits, and three G subunits. *C. elegans* encodes two B subunits, VHA-12 and SPE-5, and two H subunits. The existence of multiple subunit isoforms may tune V-ATPase activity or confer additional functions independent of proton pumping. This is clearly the case for different subunit *a* V_o isoforms in yeast; proton coupling to ATPase hydrolysis is weaker in the Golgi-specific isoform than in the vacuole-specific isoform (Kawasaki-Nishi *et al.* 2001a,b). Also, as discussed above, synaptic vesicle V_o subunit *a1* isoform may have a fusogenic role distinct from its function in pumping protons (Morel *et al.* 2003; Hiesinger *et al.* 2005; Di Giovanni *et al.* 2010).

Do V_1 subunit isoforms similarly tune V-ATPases or confer additional functions? Or is there another explanation for subunit diversity? In mammals, the B1 isoform secretes protons into the lumen of excretory ducts, and the B2 subunit acidifies organelles (Brown *et al.* 2009). Because B2 can partially substitute for B1 function in kidneys (Păunescu *et al.* 2007), and B2 isoforms are found on the surface osteoclasts (Lee *et al.* 1996), it is not clear whether the presence of either isoform changes the activity of the V-ATPase. Although *C. elegans* contains two B subunit paralogs, our functional and expression pattern analyses suggest that VHA-12 is required in essentially every somatic *C. elegans* cell. By contrast, SPE-5 seems to be largely limited to a requirement in sperm (Gleason *et al.* 2012). It is possible that SPE-5 confers specialized attributes or regulation to the V_1 sector in sperm. However, VHA-12 can at least partially compensate for loss of SPE-5 (Gleason *et al.* 2012).

An alternative reason for the duplication of B subunit genes is not to modify V-ATPase function by incorporating different subunit variants, but rather simply to escape epigenetic chromosome inactivation mechanisms. The *vha-12* gene is on the X chromosome and the *spe-5* gene is on an autosome (Gleason *et al.* 2012). The X chromosome exhibits complex expression patterns in the germ line. The X chromosome is largely silenced in the distal gonad in the female germ line (Reinke *et al.* 2000; Kelly *et al.* 2002). However, the female germ line and oocytes do not appear to possess acidified organelles, so *vha-12* expression in the mitotic germ cells might not be required (Kostich *et al.* 2000). On the other hand, we found that *vha-12* function is required in the female germ line for viability during the very early divisions of the embryo. This requirement is fully consistent with the activation of expression from the X chromosome in late pachytene of oocytes (Reinke *et al.* 2000; Kelly *et al.* 2002). *vha-12* is expressed during oogenesis (Wang *et al.* 2009) and these maternally expressed transcripts are observed in early embryos (Figure S5) (Shin-i and Kohara 2005). Although oocytes appear not to possess acidic compartments, acidified compartments are required soon after fertilization to degrade paternal mitochondria (Al Rawi *et al.* 2011; Sato and Sato 2011; Zhou *et al.* 2011). Thus, portions of the X chromosome, including *vha-12*, must be reactivated during meiosis despite chromosome condensation in pachytene to prepare for proliferative stages of embryogenesis.

The X chromosome does not reactivate in the male germ line. The X chromosome is inactivated during gonadogenesis in hermaphrodites and males (Reinke *et al.* 2000; Kelly *et al.* 2002) and X chromosomes derived from males may remain silenced even after fertilization (Bean *et al.* 2004). Consistent with this pattern of silencing, sperm-enriched genes are nearly completely absent from the X chromosome (Reinke *et al.* 2000). By contrast, the membranous organelles of spermatocytes must be acidified to generate functional sperm. As proposed by Gleason *et al.* (2012), the presence of *spe-5* on an autosome might circumvent the effects of X chromosome inactivation during spermatogenesis. In fact there are only two V_1 subunits in the *C. elegans* genome that have multiple subunit isoforms, subunit B and subunit H, and each of these subunits has one isoform on the X chromosome. Thus, it is possible that there are not specialized V_1 sectors, but rather they all function identically; gene duplication is simply a means to ensure expression in the face of X chromosome silencing.

Acknowledgments

We thank H. Robert Horvitz, in whose laboratory the *n2915* mutant was isolated, and Josh Kaplan for help during the screen; Gary Ruvkun, in whose laboratory the allele *mg41* was isolated; Steve L'Hernault, for sharing unpublished results; and Andy Fire and Christian Frøkjær-Jensen for plasmids. We thank Aude Ada-Nguema, Zheng Zhou, Gillian Stanfield, and Greg Hermann, who provided advice. We also thank Seongseop Kim, for photography assistance. G.G.E. received a National Research Service Award from the National Institutes of Health (NIH), NINDS section. Funding for this work was from NIH grants NS034307, GM65115, and GM57173.

Note added in proof: See E. J. Gleason *et al.* (pp. 477–491) in this issue, for a related work.

Literature Cited

Abrahams, J. P., A. G. Leslie, R. Lutter, and J. E. Walker, 1994 Structure at 2.8 Å resolution of F1-ATPase from bovine heart mitochondria. Nature 370: 621–628.

Al Rawi, S., S. Louvet-Vallée, A. Djeddi, M. Sachse, E. Culetto *et al.*, 2011 Postfertilization autophagy of sperm organelles prevents paternal mitochondrial DNA transmission. Science 334: 1144–1147.

Bean, C. J., C. E. Schaner, and W. G. Kelly, 2004 Meiotic pairing and imprinted X chromatin assembly in *Caenorhabditis elegans*. Nat. Genet. 36: 100–105.

Bembenek, J. N., C. T. Richie, J. M. Squirrell, J. M. Campbell, K. W. Eliceiri *et al.*, 2007 Cortical granule exocytosis in *C. elegans* is regulated by cell cycle components including separase. Development 134: 3837–3848.

Brenner, S., 1974 The genetics of *Caenorhabditis elegans*. Genetics 77: 71–94.

Brown, D., T. G. Păunescu, S. Breton, and V. Marshansky, 2009 Regulation of the V-ATPase in kidney epithelial cells: dual role in acid-base homeostasis and vesicle trafficking. J. Exp. Biol. 212: 1762–1772.

Clark, S. G., X. Lu, and H. R. Horvitz, 1994 The *Caenorhabditis elegans* locus *lin-15*, a negative regulator of a tyrosine kinase signaling pathway, encodes two different proteins. Genetics 137: 987–997.

Conradt, B., and D. Xue, 2005 Programmed cell death (October 6, 2005). WormBook, ed. The *C. elegans* Research Community, WormBook, doi/10.1895/wormbook.1.32.1, http://www.wormbook.org.

Davies, S. A., S. F. Goodwin, D. C. Kelly, Z. Wang, M. A. Sözen *et al.*, 1996 Analysis and inactivation of *vha55*, the gene encoding the vacuolar ATPase B-subunit in *Drosophila melanogaster* reveals a larval lethal phenotype. J. Biol. Chem. 271: 30677–30684.

Dettmer, J., A. Hong-Hermesdorf, Y.-D. Stierhof, and K. Schumacher, 2006 Vacuolar H^+-ATPase activity is required for endocytic and secretory trafficking in *Arabidopsis*. Plant Cell 18: 715–730.

Di Giovanni, J., S. Boudkkazi, S. Mochida, A. Bialowas, N. Samari *et al.*, 2010 V-ATPase membrane sector associates with synaptobrevin to modulate neurotransmitter release. Neuron 67: 268–279.

Dou, H. D., K. F. Finberg, E. L. Cardell, R. L. Lifton, and D. C. Choo, 2003 Mice lacking the B1 subunit of H^+-ATPase have normal hearing. Hear. Res. 180: 76–84.

Du, J., L. Kean, A. K. Allan, T. D. Southall *et al.*, 2006 The *SzA* mutations of the B subunit of the *Drosophila* vacuolar H^+ ATPase identify conserved residues essential for function in fly and yeast. J. Cell Sci. 119: 2542–2551.

Ellis, H. M., and H. R. Horvitz, 1986 Genetic control of programmed cell death in the nematode C. elegans. Cell 44: 817–829.

Finberg, K. E., C. A. Wagner, M. A. Bailey, T. G. Păunescu, S. Breton *et al.*, 2005 The B1-subunit of the H^+ ATPase is required for maximal urinary acidification. Proc. Natl. Acad. Sci. USA 102: 13616–13621.

Forgac, M., 2007 Vacuolar ATPases: rotary proton pumps in physiology and pathophysiology. Nat. Rev. Mol. Cell Biol. 8: 917–929.

Fuster, D. G., J. Zhang, X. S. Xie, and O. W. Moe, 2008 The vacuolar-ATPase B1 subunit in distal tubular acidosis: novel mutations and mechanisms for dysfunction. Kidney Int. 73: 1151–1158.

Futai, M., T. Oka, G. Sun-Wada, Y. Moriyama, H. Kanazawa *et al.*, 2000 Luminal acidification of diverse organelles by V-ATPase in animal cells. J. Exp. Biol. 203: 107–116.

Gil, H., F. Santos, E. García, M. V. Alvarez, F. A. Ordóñez *et al.*, 2007 Distal RTA with nerve deafness: clinical spectrum and mutational analysis in five children. Pediatr. Nephrol. 22: 825–828.

Gleason, E. J., P. D. Hartley, M. Henderson, K. L. Hill-Harfe, P. W. Price *et al.*, 2012 Developmental genetics of secretory vesicle acidification during *Caenorhabditis elegans* spermatogenesis. Genetics 191: 477–491.

Hahn, H., H. G. Kang, I. S. Ha, H. I. Cheong, and Y. Choi, 2003 ATP6B1 gene mutations associated with distal renal tubular acidosis and deafness in a child. Am. J. Kidney Dis. 41: 238–243.

He, B., N. Lu, and Z. Zhou, 2009 Cellular and nuclear degradation during apoptosis. Curr. Opin. Cell Biol. 21: 900–912.

Hiesinger, P. R., A. Fayyazuddin, S. Q. Mehta, T. Rosenmund, K. L. Schulze *et al.*, 2005 The v-ATPase V0 subunit *a1* is required for a late step in synaptic vesicle exocytosis in *Drosophila*. Cell 121: 607–620.

Hurtado-Lorenzo, A., M. Skinner, J. El Annan, M. Futai, G.-H. Sun-Wada *et al.*, 2006 V-ATPase interacts with ARNO and Arf6 in early endosomes and regulates the protein degradative pathway. Nat. Cell Biol. 8: 124–136.

Jorgensen, E. M., E. Hartwieg, K. Schuske, M. L. Nonet, Y. Jin *et al.*, 1995 Defective recycling of synaptic vesicles in synaptotagmin mutants of *Caenorhabditis elegans*. Nature 378: 196–199.

Kane, P. M., 2006 The where, when, and how of organelle acidification by the yeast vacuolar H^+-ATPase. Microbiol. Mol. Biol. Rev. 70: 177–191.

Karet, F. E., K. E. Finberg, R. D. Nelson, A. Nayir, H. Mocan *et al.*, 1999 Mutations in the gene encoding B1 subunit of H^+-ATPase cause renal tubular acidosis with sensorineural deafness. Nat. Genet. 21: 84–90.

Kawasaki-Nishi, S., K. Bowers, T. Nishi, M. Forgac, and T. H. Stevens, 2001a The amino-terminal domain of the vacuolar proton-translocating ATPase a subunit controls targeting and in vivo dissociation, and the carboxyl-terminal domain affects coupling of proton transport and ATP hydrolysis. J. Biol. Chem. 276: 47411–47420.

Kawasaki-Nishi, S., T. Nishi, and M. Forgac, 2001b Yeast V-ATPase complexes containing different isoforms of the 100-kDa a-subunit differ in coupling efficiency and *in vivo* dissociation. J. Biol. Chem. 276: 17941–17948.

Kelly, W. G., C. E. Schaner, A. F. Dernburg, M. H. Lee, S. K. Kim *et al.*, 2002 X-chromosome silencing in the germline of *C. elegans*. Development 129: 479–492.

Kostich, M., A. Fire, and D. M. Fambrough, 2000 Identification and molecular-genetic characterization of a LAMP/CD68-like protein from *Caenorhabditis elegans*. J. Cell Sci. 113(Pt. 14): 2595–2606.

Lee, B. S., L. S. Holliday, B. Ojikutu, I. Krits, and S. L. Gluck, 1996 Osteoclasts express the B2 isoform of vacuolar H^+-ATPase intracellularly and on their plasma membranes. Am. J. Physiol. 270: C382–C388.

Lee, J. H., W. H. Yu, A. Kumar, S. Lee, P. S. Mohan *et al.*, 2010 Lysosomal proteolysis and autophagy require presenilin 1 and are disrupted by Alzheimer-related PS1 mutations. Cell 141: 1146–1158.

Lee, S. K., W. Li, S. E. Ryu, T. Rhim, and J. Ahnn, 2010 Vacuolar H^+-ATPases in *Caenorhabditis elegans*: What can we learn about giant H^+ pumps from tiny worms? Biochim. Biophys. Acta 1797: 1687–1695.

Liégeois, S., A. Benedetto, J. M. Garnier, Y. Schwab, and M. Labouesse, 2006 The V0-ATPase mediates apical secretion of exosomes containing Hedgehog-related proteins in *Caenorhabditis elegans*. J. Cell Biol. 173: 949–961.

Liu, Q., P. M. Kane, P. R. Newman, and M. Forgac, 1996 Site-directed mutagenesis of the yeast V-ATPase B subunit (Vma2p). J. Biol. Chem. 271: 2018.

McDonald, K., H. Schwarz, T. Müller-Reichert, R. Webb, C. Buser *et al.*, 2010 "Tips and tricks" for high-pressure freezing of model systems. Methods Cell Biol. 96: 671–693.

McIntire, S. L., R. J. Reimer, K. Schuske, R. H. Edwards, and E. M. Jorgensen, 1997 Identification and characterization of the vesicular GABA transporter. Nature 389: 870–876.

McMahon, L., J. M. Muriel, B. Roberts, M. Quinn, and I. L. Johnstone, 2003 Two sets of interacting collagens form functionally distinct substructures within a *Caenorhabditis elegans* extracellular matrix. Mol. Biol. Cell 14: 1366–1378.

Mellman, I., R. Fuchs, and A. Helenius, 1986 Acidification of the endocytic and exocytic pathways. Annu. Rev. Biochem. 55: 663–700.

Miesenböck, G., D. A. De Angelis, and J. E. Rothman, 1998 Visualizing secretion and synaptic transmission with pH-sensitive green fluorescent proteins. Nature 394: 192–195.

Miller, K. G., A. Alfonso, M. Nguyen, J. A. Crowell, C. D. Johnson *et al.*, 1996 A genetic selection for *Caenorhabditis elegans* synaptic transmission mutants. Proc. Natl. Acad. Sci. USA 93: 12593–12598.

Morel, N., J. C. Dedieu, and J. M. Philippe, 2003 Specific sorting of the *a1* isoform of the V-H^+ATPase a subunit to nerve terminals where it associates with both synaptic vesicles and the presynaptic plasma membrane. J. Cell Sci. 116: 4751–4762.

Nishi, T., and M. Forgac, 2002 The vacuolar H^+-ATPases–nature's most versatile proton pumps. Nat. Rev. Mol. Cell Biol. 3: 94–103.

Oka, T., T. Toyomura, K. Honjo, Y. Wada, and M. Futai, 2001 Four subunit *a* isoforms of *Caenorhabditis elegans* vacuolar H^+-ATPase. Cell-specific expression during development. J. Biol. Chem. 276: 33079–33085.

Orlowski, J., and S. Grinstein, 2007 Emerging roles of alkali cation/proton exchangers in organellar homeostasis. Curr. Opin. Cell Biol. 19: 483–492.

Page, A., and I. L. Johnstone, 2007 The cuticle (March 19, 2007), *WormBook*, ed. The *C. elegans* Research Community, WormBook, doi/10.1895/wormbook.1.138.1, http://www.wormbook.org.

Păunescu, T. G., L. M. Russo, N. Da Silva, J. Kovacikova, N. Mohebbi *et al.*, 2007 Compensatory membrane expression of the V-ATPase B2 subunit isoform in renal medullary intercalated cells of B1-deficient mice. Am. J. Physiol. Renal Physiol. 293: F1915–F1926.

Peri, F., and C. Nüsslein-Volhard, 2008 Live imaging of neuronal degradation by microglia reveals a role for v0-ATPase a1 in phagosomal fusion in vivo. Cell 133: 916–927.

Peters, C., M. J. Bayer, S. Bühler, J. S. Andersen, M. Mann *et al.*, 2001 Trans-complex formation by proteolipid channels in the terminal phase of membrane fusion. Nature 409: 581–588.

Pujol, N., C. Bonnerot, J. J. Ewbank, Y. Kohara, and D. Thierry-Mieg, 2001 The *Caenorhabditis elegans unc-32* gene encodes alternative forms of a vacuolar ATPase *a* subunit. J. Biol. Chem. 276: 11913–11921.

Ramot, D., B. E. Johnson, T. L. Berry, L. Carnell, and M. B. Goodman, 2008 The Parallel Worm Tracker: a platform for measuring average speed and drug-induced paralysis in nematodes. PLoS ONE 3: e2208.

Reinke, V., H. E. Smith, J. Nance, J. Wang, C. Van Doren *et al.*, 2000 A global profile of germline gene expression in *C. elegans*. Mol. Cell 6: 605–616.

Rostaing, P., R. M. Weimer, E. M. Jorgensen, A. Triller, and J. L. Bessereau, 2004 Preservation of immunoreactivity and fine structure of adult *C. elegans* tissues using high-pressure freezing. J. Histochem. Cytochem. 52: 1–12.

Sankaranarayanan, S., D. De Angelis, J. E. Rothman, and T. A. Ryan, 2000 The use of pHluorins for optical measurements of presynaptic activity. Biophys. J. 79: 2199–2208.

Sato, M., and K. Sato, 2011 Degradation of paternal mitochondria by fertilization-triggered autophagy in *C. elegans* embryos. Science 334: 1141–1144.

Sato, M., B. D. Grant, A. Harada, and K. Sato, 2008 Rab11 is required for synchronous secretion of chondroitin proteoglycans after fertilization in *Caenorhabditis elegans*. J. Cell Sci. 121: 3177–3186.

Shin-i, T., and Y. Kohara, 2005 The Nematode Expression Pattern Database, NEXTDB ver. 4. Available at http://nematode.lab.nig.ac.jp/. Accessed January 23, 2012.

Stover, E. H., K. J. Borthwick, C. Bavalia, N. Eady, D. M. Fritz *et al.*, 2002 Novel ATP6V1B1 and ATP6V0A4 mutations in autosomal recessive distal renal tubular acidosis with new evidence for hearing loss. J. Med. Genet. 39: 796–803.

Strasser, B., J. Iwaszkiewicz, O. Michielin, and A. Mayer, 2011 The V-ATPase proteolipid cylinder promotes the lipid-mixing stage of SNARE-dependent fusion of yeast vacuoles. EMBO J. 30: 4126–4141.

Sulston, J. E., and S. Brenner, 1974 The DNA of *Caenorhabditis elegans*. Genetics 77: 95–104.

Sulston, J. E., E. Schierenberg, J. G. White, and J. N. Thomson, 1983 The embryonic cell lineage of the nematode *Caenorhabditis elegans*. Dev. Biol. 100: 64–119.

Sun-Wada, G. H., T. Toyomura, Y. Murata, A. Yamamoto, M. Futai *et al.*, 2006 The *a3* isoform of V-ATPase regulates insulin secretion from pancreatic beta-cells. J. Cell Sci. 119: 4531–4540.

Toei, M., R. Saum, and M. Forgac, 2010 Regulation and isoform function of the V-ATPases. Biochemistry 49: 4715–4723.

Vargas-Poussou, R., P. Houillier, N. Le Pottier, L. Strompf, C. Loirat *et al.*, 2006 Genetic investigation of autosomal recessive distal renal tubular acidosis: evidence for early sensorineural hearing loss associated with mutations in the ATP6V0A4 gene. J. Am. Soc. Nephrol. 17: 1437–1443.

Wang, X., Y. Zhao, K. Wong, P. Ehlers, Y. Kohara *et al.*, 2009 Identification of genes expressed in the hermaphrodite germ line of *C. elegans* using SAGE. BMC Genomics 10: 213.

Williamson, W. R., D. Wang, A. S. Haberman, and P. R. Hiesinger, 2010 A dual function of V0-ATPase *a1* provides an endolysosomal degradation mechanism in *Drosophila melanogaster* photoreceptors. J. Cell Biol. 189: 885–899.

Yochem, J., and R. K. Herman, 2003 Investigating *C. elegans* development through mosaic analysis. Development 130: 4761–4768.

Yochem, J., T. Gu, and M. Han, 1998 A new marker for mosaic analysis in *Caenorhabditis elegans* indicates a fusion between hyp6 and hyp7, two major components of the hypodermis. Genetics 149: 1323–1334.

Yu, X., S. Odera, C. H. Chuang, N. Lu, and Z. Zhou, 2006 *C. elegans* dynamin mediates the signaling of phagocytic receptor CED-1 for the engulfment and degradation of apoptotic cells. Dev. Cell 10: 743–757.

Yuan, J., S. Shaham, S. Ledoux, H. M. Ellis, and H. R. Horvitz, 1993 The *C. elegans* cell death gene *ced-3* encodes a protein similar to mammalian interleukin-1β-converting enzyme. Cell 75: 641–652.

Zhou, Q., H. Li, and D. Xue, 2011 Elimination of paternal mitochondria through the lysosomal degradation pathway in *C. elegans*. Cell Res. 21: 1662–1669.

Communicating editor: O. Hobert

GENETICS

Supporting Information
http://www.genetics.org/content/suppl/2012/03/16/genetics.112.139667.DC1

V-ATPase V_1 Sector Is Required for Corpse Clearance and Neurotransmission in *Caenorhabditis elegans*

Glen G. Ernstrom, Robby Weimer, Divya R. L. Pawar, Shigeki Watanabe, Robert J. Hobson, David Greenstein, and Erik M. Jorgensen

DOI: 10.1534/genetics.112.139667

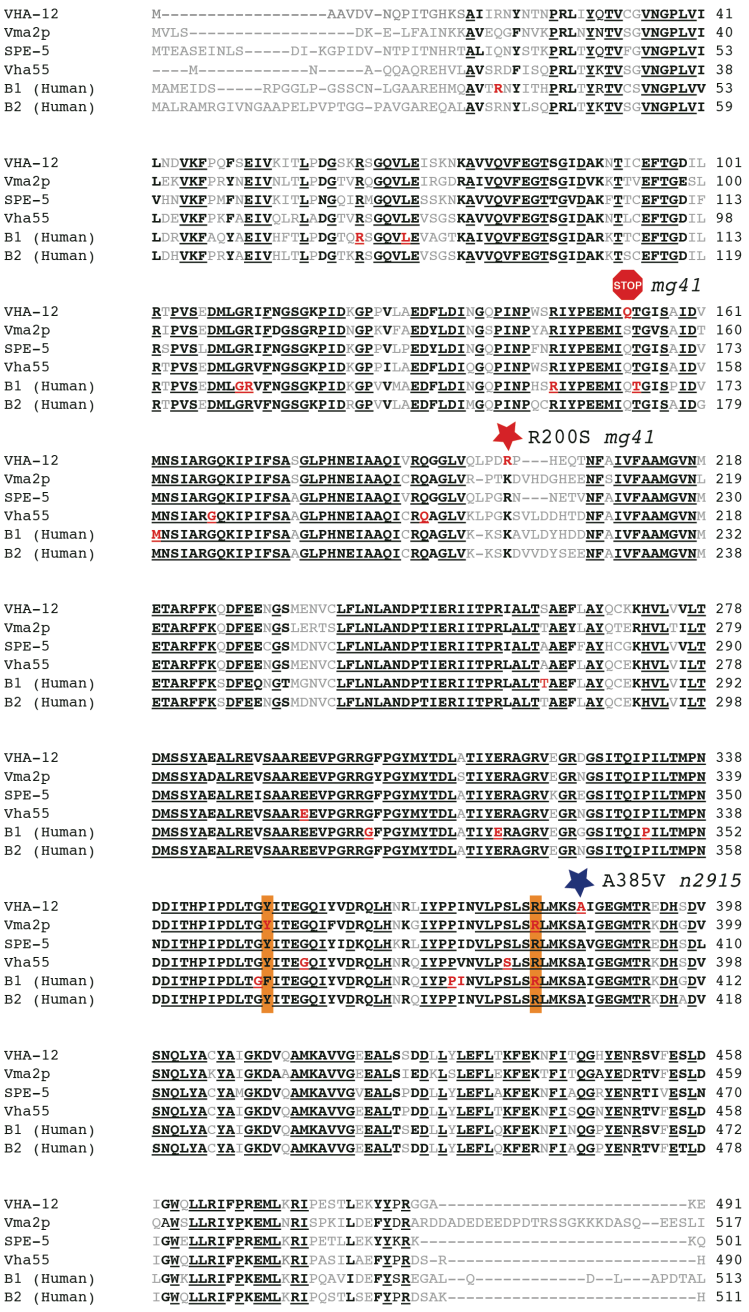

Figure S1 Sequence alignment of the VHA-12 polypeptide. V-ATPase B subunits exhibit high sequence identity to *C. elegans* VHA-12, including yeast Vma2p (70.2%), *C. elegans* SPE-5 (82.5%), *Drosophila* Vha55 (84.2%), and human B1 (78.4%) and B2 (80.7%) (alignments using T-COFFEE, Notredame *et al.*, 2000) sequence identity using NEEDLE. Identical and similar resides are bold black with identities underlined. Non-conserved residues are gray. Red residues indicate point mutations that cause loss-of-function mutations in the respective organisms. Human B1 subunit mutations are linked to distal renal tubule acidosis sometimes also associated with sensorineural deafness. The orange stripe corresponds to highly conserved residues that are required for Vma2p function and likely contribute directly to ATP catalysis. Non-VHA-12 mutant allele information was gathered from Liu et al., 1996 (Yeast); Du *et al.,* 2006 (*Drosophila*); Human: Karet *et al.*, 1999; Stover *et al.,* 2002; Hahn *et al.,* 2003*;* Vargas-Poussou *et al.,* 2006*;* Gil *et al., 2007*; and Fuster *et al.,* 2008.

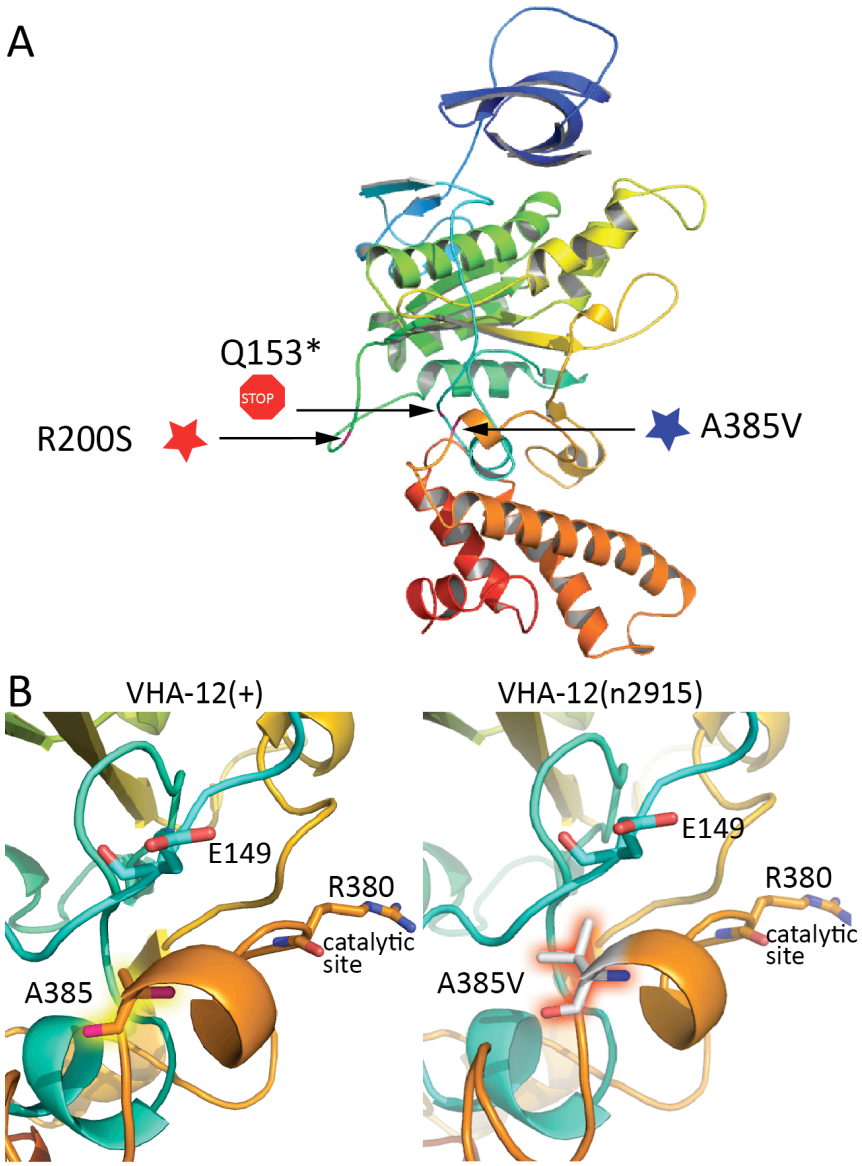

Figure S2 A homology model of VHA-12. (A) Shown is the three-dimensional homology model of VHA-12 generated using the template of the crystal structure of the B subunit of the A-ATPase from *Methanosarcina mazei* Gö1 (PDB: 2c61 chain A) (Schäfer *et al.*, 2006). The model was generated in SWISS-MODEL in conjunction with DEEPVIEW in project mode (Arnold *et al.*, 2006). Positions of *vha-12(mg41)*, red, and *vha-12(n2915)* lesions, blue, are shown. (B) Detail of the predicted catalytic site indicating the location of the critical arginine (R380) likely to directly participate in ATP catalysis. Alanine 385 (A385) is mutated to a valine in VHA-12(n2915). In the model, alanine 385 is opposite a conserved glutamate (E149) (residue shown in blue) that is polymorphic in humans (E161K). The E161K form is subfunctional in heterologous assays, but can assemble with other V-ATPase subunits (Fuster *et al.*, 2008).

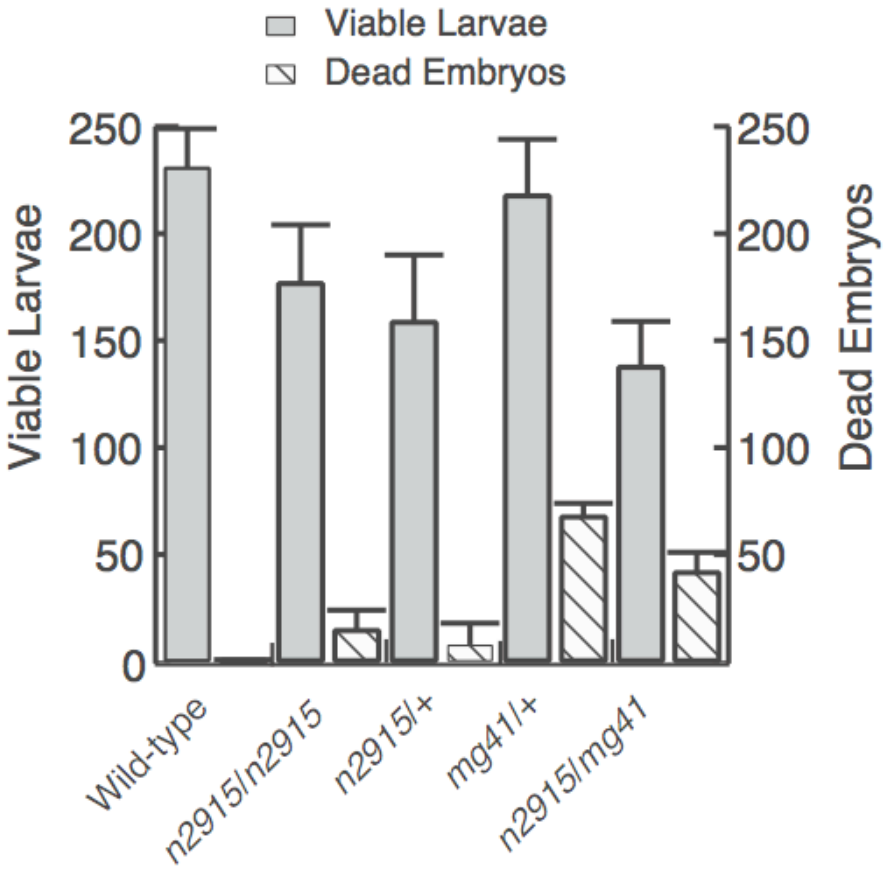

Figure S3 Fecundity and embryonic lethality. Wild-type animals laid an average 231±18 (mean±SD) embryos in each brood that hatched to produce viable larvae. A dead wild-type embryo was rare (0.25±0.71 per brood). *n2915* homozygotes laid 192 total embryos per brood, 177±27 embryos hatched to produce viable larvae and 15±9 embryos died in each brood. The total embryos laid by *vha-12(mg41)/+* (285 embryos) was not decreased compared to the wild type. Embryonic lethality. In contrast to the wild type, some embryos from *vha-12(n2915)* homozygotes and heterozygotes died (15 and 8 dead embryos, respectively). *vha-12(mg41)/+* hermaphrodites produced 1/4 dead embryos (138 hatched larvae: 42 dead embryos), as expected for a recessive lethal allele. Bars represent mean±SD of 3-8 independent measurements.

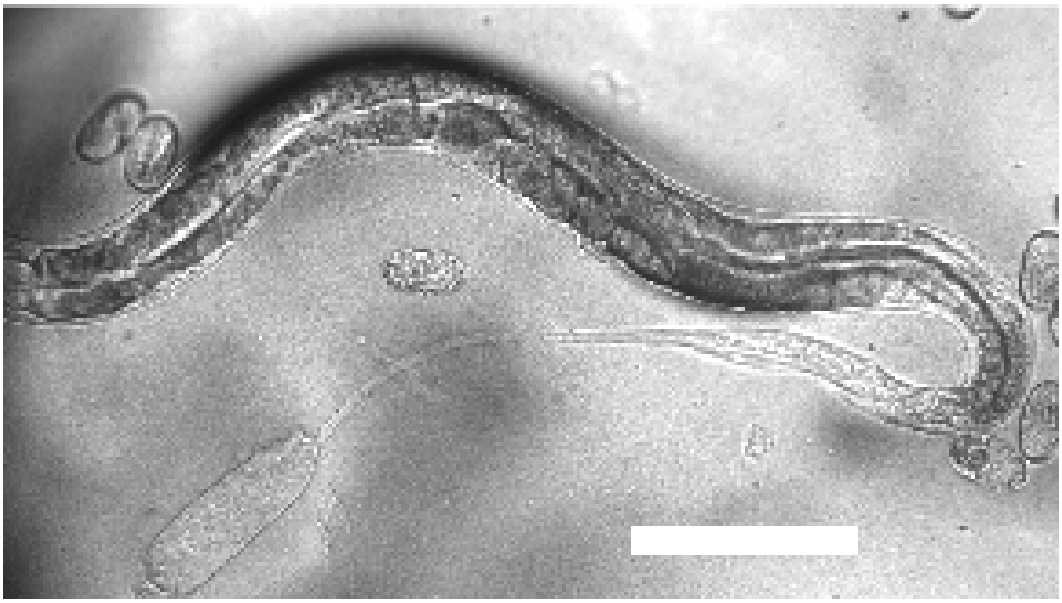

Figure S4 Molting defect. A representative one-day old *vha-12(n2915)/+* dragging cuticle from its tail from a previous molt. Scale bar = 0.1 mm.

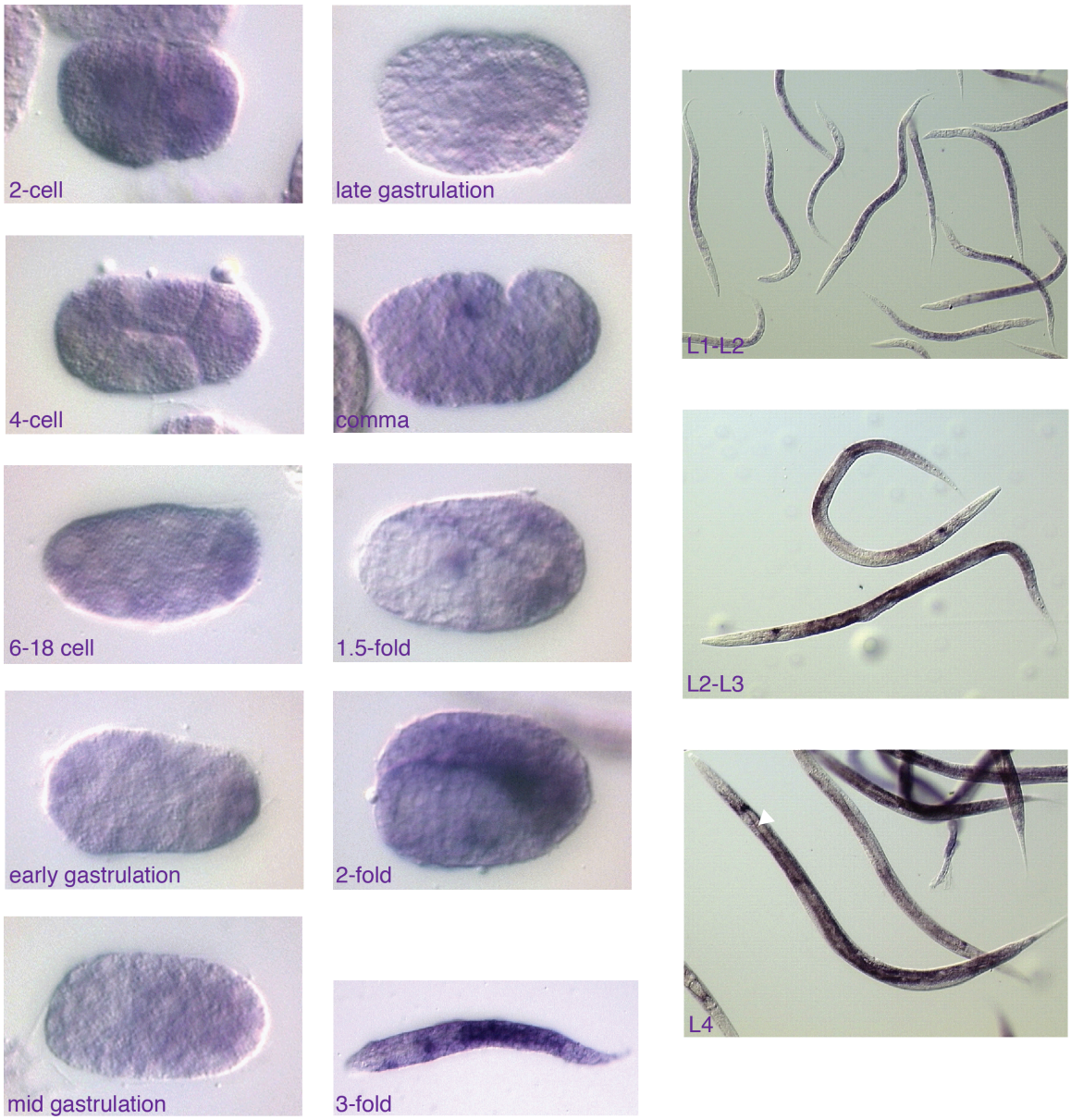

Figure S5 *vha-12* in situ hybridization. *vha-12* transcripts are detected as early as the 2-cell stage in developing embryos. Strong staining is observed in the developing gut from mid-gastrulation through the 1.5-fold stage. H-shaped excretory cell in L4 larvae (white arrow). Images reproduced with permission from Kohara, Y. (NEXTDB ver. 4 clone 102c11 http://nematode.lab.nig.ac.jp/).

File S1

Wild-type corpse clearance

File S1 is available for download as a QuickTime movie file at http://www.genetics.org/. A representative movie tracking a wild-type apoptotic cell corpse (white box). Note the time index is the elapsed time from the start of the movie acquisition shown in File S5, not the time after first cleavage.

File S2

Corpse clearance in *vha-12(mg41)* mutant

File S2 is available for download as a QuickTime movie file at http://www.genetics.org/. A representative movie tracking an apoptotic cell corpse (white box) in a *vha-12(mg41)* mutant embryo that later developmentally arrested and died. Note the time index is the elapsed time from the start of the movie acquisition shown in File S6, not the time after first cleavage.

File S3

Wild-type corpse clearance image stack

File S3 is available for download as a QuickTime movie file at http://www.genetics.org/. A representative movie tracking a wild-type apoptotic corpse (white box). In this movie (the same embryo in File S1), three focal planes above the corpse, and three focal planes below the corpse at each time interval is shown. Note the time index is the elapsed time from the start of the movie acquisition shown in File S5, not the time after first cleavage.

File S4

Corpse clearance in a *vha-12(mg41)* mutant imaging stack

File S4 is available for download as a QuickTime movie file at http://www.genetics.org. A representative movie tracking an apoptotic cell corpse (white box) in a *vha-12(mg41)* mutant embryo that later developmentally arrested and died. In this movie (the same embryo in File S2), three focal planes above the corpse, and three focal planes below the corpse at each time interval is shown. Note the time index is the elapsed time from the start of the movie acquisition shown in File S6, not the time after first cleavage.

File S5

Wild-type embryonic development

File S5 is available for download as a QuickTime movie file at http://www.genetics.org. A representative movie of wild-type (N2) embryonic development captured on our imaging system.

File S6

vha-12(mg41)/vha-12(mg41) development from vha-12(mg41); mnDp31 parent

File S6 is available for download as a QuickTime movie file at http://www.genetics.org. A representative movie of a *vha-12(mg41)* mutant embryo that lost the free duplication that balances the lethal mutation (the neighboring embryo to the left still carries the wild-type duplication).

LITERATURE CITED

Arnold, K., L. Bordoli, J. Kopp, and T. Schwede, 2006 The SWISS-MODEL workspace: a web-based environment for protein structure homology modelling. Bioinformatics **22:** 195-201.

Du, J., L. Kean, A. K. Allan, T. D. Southall, *et al.*, 2006 The *SzA* mutations of the B subunit of the *Drosophila* vacuolar H^+ ATPase identify conserved residues essential for function in fly and yeast. J Cell Sci **119:** 2542-2551.

Fuster, D. G., J. Zhang, X. S. Xie, and O. W. Moe, 2008 The vacuolar-ATPase B1 subunit in distal tubular acidosis: novel mutations and mechanisms for dysfunction. Kidney Int **73:** 1151-1158.

Gil, H., F. Santos, E. García, M. V. Alvarez, *et al.*, 2007 Distal RTA with nerve deafness: clinical spectrum and mutational analysis in five children. Pediatr Nephrol **22:** 825-828.

Hahn, H., H. G. Kang, I. S. Ha, H. I. Cheong, and Y. Choi, 2003 ATP6B1 gene mutations associated with distal renal tubular acidosis and deafness in a child. Am J Kidney Dis **41:** 238-243.

Karet, F. E., K. E. Finberg, R. D. Nelson, A. Nayir, *et al.*, 1999 Mutations in the gene encoding B1 subunit of H^+-ATPase cause renal tubular acidosis with sensorineural deafness. Nat Genet **21:** 84-90.

Liu, Q., P. M. Kane, P. R. Newman, and M. Forgac, 1996 Site-directed mutagenesis of the yeast V-ATPase B subunit (Vma2p). J Biol Chem **271:** 2018.

Notredame, C., D. G. Higgins, and J. Heringa, 2000 T-Coffee: A novel method for fast and accurate multiple sequence alignment. J Mol Biol **302:** 205-217.

Schäfer, I. B., S. M. Bailer, M. G. Düser, M. Börsch, *et al.*, 2006 Crystal structure of the archaeal A1Ao ATP synthase subunit B from Methanosarcina mazei Gö1: Implications of nucleotide-binding differences in the major A1Ao subunits A and B. J Mol Biol **358:** 725-740.

Stover, E. H., K. J. Borthwick, C. Bavalia, N. Eady, *et al.*, 2002 Novel ATP6V1B1 and ATP6V0A4 mutations in autosomal recessive distal renal tubular acidosis with new evidence for hearing loss. J Med Genet **39:** 796-803.

Vargas-Poussou, R., P. Houillier, N. Le Pottier, L. Strompf, *et al.*, 2006 Genetic investigation of autosomal recessive distal renal tubular acidosis: evidence for early sensorineural hearing loss associated with mutations in the ATP6V0A4 gene. J Am Soc Nephrol **17:** 1437-1443.